This document is the accepted manuscript version of the following article:
Trachsel, L., Romio, M., Grob, B., Zenobi-Wong, M., Spencer, N. D., Ramakrishna, S. N., & Benetti, E. M. (2020). Functional nanoassemblies of cyclic polymers show amplified responsiveness and enhanced protein-binding ability. ACS Nano, 14(8), 10054-10067. https://doi.org/10.1021/acsnano.0c03239

Functional Nanoassemblies of Cyclic Polymers Show Amplified Responsiveness and Enhanced Protein-Binding Ability

Lucca Trachsel,[1] Matteo Romio,[2,3] Benjamin Grob,[3] Marcy Zenobi-Wong,[1] Nicholas D. Spencer,[3] Shivaprakash N. Ramakrishna,[3]* Edmondo M. Benetti[2,3]**

1) Tissue Engineering + Biofabrication Laboratory, Department of Health Sciences and Technology, ETH Zürich, 8093 Zürich, Switzerland, Email: marcy.zenobi@hest.ethz.ch

2) Biointerfaces, Swiss Federal Laboratories for Materials Science and Technology (Empa), Lerchenfeldstrasse 5, CH-9014, St. Gallen, Switzerland

3) Laboratory for Surface Science and Technology, Department of Materials, ETH Zürich; Vladimir-Prelog-Weg 5, 8093 Zürich, Email: nspencer@ethz.ch; shivaprakash.ramakrishna@mat.ethz.ch; edmondo.benetti@mat.ethz.ch

ABSTRACT

The physicochemical properties of cyclic polymer adsorbates are significantly influenced by the steric and conformational constraints introduced during their cyclization. These translate into a marked difference in interfacial properties between cyclic polymers and their linear counterparts, when they are grafted onto surfaces yielding nanoassemblies or polymer brushes. This difference is particularly clear in the case of cyclic polymer brushes that are designed to chemically interact with the surrounding environment, for instance by associating with biological components present in the medium, or, alternatively, through a response to a chemical stimulus by a significant change in their properties.

The intrinsic architecture characterizing cyclic poly(2-oxazoline)-based polyacid brushes leads to a broad variation in swelling and nanomechanical properties in response to pH change, in comparison to their linear analogues of identical composition and molecular weight. In addition, cyclic glycopolymer brushes derived from polyacids reveal an enhanced exposure of galactose units at the surface, due to their expanded topology, and thus display an increased lectin-binding ability with respect to their linear counterparts.

This combination of amplified responsiveness and augmented protein-binding capacity renders cyclic brushes invaluable building blocks for the design of “smart” materials and functional biointerfaces.

KEYWORDS: polymer topology; cyclic polymers; polymer brushes; nanofilms; atomic force microscopy.

During the last decade, a variety of synthetic paths have been successfully established to produce cyclic polymers with high purity and in good yield, including ring-closure strategies starting from chain-end functional precursors,[1-3] and ring-expansion techniques that have exploited cyclic precursors and/or catalysts.[4-8] Simultaneously, experimentalists and theoreticians have progressively demonstrated that topology effects in cyclic macromolecules substantially alter several fundamental physicochemical properties in bulk, melts and solutions, such as molecular dimensions,[9-12] rheological characteristics[13] and solvation properties.[14-17]

From this starting point, increasing efforts have been recently devoted to applying the distinctive properties of cyclic polymers in materials science, in an effort to translate a polymer class that was defined as little more than a scientific curiosity into building blocks for the formulation of advanced materials.[18]

We have specifically focused on the application of cyclic polymers to generate interfaces with broadly tunable properties on organic and inorganic supports, and nanoparticles (NPs).[19] On macroscopic surfaces, the exceptional steric stabilization and molecular compactness provided by cyclic macromolecules, coupled with their intrinsic absence of chain ends, can generate nanofilms with distinctive biopassive, and tribological properties. In particular, cyclic poly(2-alkyl-2-oxazoline) (PAOXA) adsorbates synthesized by a ring-closure method have been applied on metal oxide substrates, as well as on cartilage, to yield polymer-brush assemblies that provide both superlubricious behavior and enhanced resistance toward nonspecific interactions with serum proteins.[20-24] Cyclic PAOXAs were additionally applied to fabricate inorganic core-cyclic polymer-shell NPs, demonstrating an excellent colloidal stability and nearly full bioinertness within aqueous media and protein dispersions.[25]

These initial studies highlighted how the intrinsic topology effects of chemically inert, cyclic macromolecules can be directly translated into a substantial modification of interfacial

physicochemical properties on solid surfaces. However, the steric and conformational constraints introduced during cyclization are additionally expected to affect the characteristics of polymer assemblies when these feature a functional character. This is the case for polymer interfaces that are chemically designed to actively interact with the surrounding environment, for instance through covalent or supramolecular associations with one or more components present in the medium, or, alternatively, through a response to a physical or chemical stimulus (such as light, or pH) by a significant change in their properties.[26]

Despite their smaller radius of hydration compared to linear analogues of similar molecular weight, cyclic polymers show an enhancement in effective intramolecular repulsion between their polymer segments. We believe that this phenomenon not only leads to a higher excluded-volume effect and greater swelling,[27] but would also generate a higher steric availability for functional groups that could not be achieved on linear polymer coils. This enhancement in the surface exposure of functionalities, simply as a result of polymer-graft chain topology, would offer an approach to the design of a large variety of reactive biointerfaces, with potential impact in drug delivery systems, bioimaging materials, and biosensors, for example.[28]

Moreover, since shifting from linear to cyclic topology can change the stimulus-responsive behavior of surface-grafted macromolecules, a more precise tuning of polymer topology could provide an additional parameter in the modulation of the properties of "smart" surfaces. While the distinctive steric restrictions characteristic of cyclic polymers have already been demonstrated to alter the temperature-induced transitions of amphiphilic polymers in solution,[29-31] the presence of a grafting surface as a boundary could further alter or amplify any physical transition. Moreover, translating similar topology effects, already observed in solution, into surface properties would enable the fabrication of responsive surfaces with

potential applications in cell-sensitive platforms,[32-34] nanostructured membranes,[35-37] or optical devices.[38-40]

Inspired by these intriguing perspectives, the objective of our study is to demonstrate that topology effects in brush-forming cyclic polymer adsorbates enable a broader tuning capability for responsive properties on surfaces, and an enhanced functional character with respect to commonly employed formulations based on linear grafts.

Linear and cyclic poly(2-carboxypropyl-2-oxazoline) (PCPOXA) adsorbates incorporating disulfide-based anchors were first synthesized by cationic ring-opening polymerization (CROP)[41] of 2-methoxycarbonylpropyl-2-oxazoline (MCPOXA),[42-43] followed by post-polymerization modification. Their subsequent assembly on Au surfaces generated topologically different, weak polyacid brushes that respond to pH by varying their swelling, nanomechanical and nanotribological properties. Through a combination of variable-angle spectroscopic ellipsometry (VASE), quartz crystal microbalance with dissipation (QCM-D) and atomic force microscopy (AFM) methods, we demonstrate that the intramolecular steric pressure generated within cyclic grafts upon deprotonation significantly alters the transition in their physicochemical properties across the pK_a. More generally, we demonstrate that the effects of polymer topology coupled with the additional constraint of a grafting surface lead to a broader response of the assemblies towards pH variation.

When the side-chain groups of PCPOXA are derivatised with galactose moieties, functional poly(2-*N*-2-deoxy-D-galactopyranosecarboxamidepropyl-2-oxazoline) (PGalaPOXA) adsorbates forming brushes can efficiently act as glycopolymer ligands for proteins.

A wide variety of cell-adhesion and recognition events, including those involved in cancer, inflammation and infection, encompass the specific interaction between carbohydrate-rich macromolecules and lectins.[44] Therefore an investigation of the effect of chain topology on

the protein-binding ability of synthetic glycopolymers on surfaces is a highly relevant approach to the development of both sensing and therapeutic materials.[45]

In the particular case of PGalaPOXA brushes, the intrinsic steric constraints present along cyclic grafts provide an augmented presentation of galactose functions at the interface, leading to a markedly higher lectin-binding efficiency with respect to linear brush analogues with similar molar mass and comparable surface coverage.

Although these results are specific for polymer surfaces that show affinity toward a particular protein type, they suggest how the translation of topology effects into interfacial properties can enhance the functional character of a large variety of reactive platforms and biomedical devices.

RESULTS AND DISCUSSION

Synthesis and Surface Assembly of Linear and Cyclic Polyacid Adsorbates on Au Surfaces

Responsive and functional polymer brushes with different chain topologies were fabricated starting from poly(2-methoxycarbonylpropyl-2-oxazoline) (PMCPOXA) species, which had been synthesized by cationic ring-opening polymerization (CROP)[41] of 2-methoxycarbonylpropyl-2-oxazoline (MCPOXA)[43] using chemically tailored initiator and terminator agents (Scheme 1a and Supporting Information). In the case of linear adsorbates, CROP was terminated by addition of piperazine, yielding PMCPOXA presenting amine chain end with M_n= 8200 Da (DP ~ 50, Supporting Information) and dispersity ($Đ$) = 1.23. Subsequent derivatization with (4-(5-(1,2-dithiolan-3-yl)pentanamido)benzoic acid) (BCLA), provided PMCPOXA with disulfide end groups that can function as specific anchors for Au surfaces (Scheme 1a and Supporting Information). Final basic hydrolysis of the methyl ester

side-chains of PMCPOXA-BCLA generated poly(2-carboxypropyl-2-oxazoline) adsorbates, yielding linear polyacid brushes on Au (*l*-PCPOXA) (Scheme 1b).

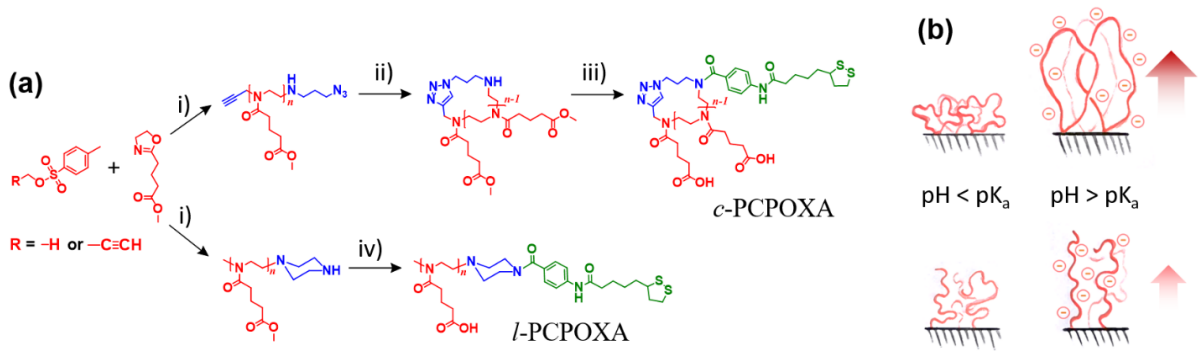

Scheme 1. (a) Synthesis of *c*-PCPOXA and *l*-PCPOXA by CROP and post-functionalization. Reaction conditions for *c*-PCPOXA are briefly summarized as follows. i) CROP: Propargyl *p*-toluenesulfonate (R=C_2H), MCPOXA, dry ACN, 80°C, 16 h under Ar; termination by 3-azidopropylamine, dry ACN, 25°C, 48 h under Ar. ii) Intramolecular cyclization using copper(I)bromide (CuBr), N,N,N',N",N"-pentamethyldiethylenetriamine (PMDETA), DCM, 25°C, 72h, under Ar. iii) BCLA, (1-cyano-2-ethoxy-2-oxoethylideneaminooxy)dimethylaminomorpholinocarbenium hexafluorophosphate (COMU), N,N-diisopropylethylamine (DIPEA), DMF, 25°C, 24 h; hydrolysis using 1M NaOH, EtOH:H_2O 2:1, 25°C, 24 h. Reaction conditions for *l*-PCPOXA. i) Methyl *p*-toluenesulfonate (R=H), MCPOXA, dry ACN, 80°C, 16 h under Ar; termination by piperazine, dry DMF, 25°C, 48 h under Ar. iv) BCLA, COMU, DIPEA, DMF, 25°C, 24 h; hydrolysis using 1M NaOH, EtOH:H_2O 2:1, 25°C, 24 h. (b) Schematic illustration depicting the pH-responsive properties by *c*-PCPOXA and *l*-PCPOXA brushes across their pK_a.

The corresponding cyclic polyelectrolyte adsorbates (*c*-PCPOXA) were synthesized following a similar general strategy. Cyclic PMCPOXA species were first obtained starting from α-alkyne-ω-azide PMCPOXA telechelic precursors with M_n = 8000 Da (DP ~ 50,

Supporting Information) and $Đ$ = 1.26. These were subjected to intramolecular cyclization by Cu(I)-catalyzed alkyne-azide cycloaddition generating cyclic PMCPOXA (Supporting Information). Subsequent functionalization with BCLA, followed by final hydrolysis of the side chains yielded *c*-PCPOXA adsorbates (Scheme 1a).

Deposition of *l*- and *c*-PCPOXA onto Au from a 10 mM methanol solution with 1 vol% acetic acid[46] generated topologically different, dense polyelectrolyte brush assemblies after just 1 h of adsorption. In particular, *l*-PCPOXA brushes showed an average dry thickness (T_{dry}) of 3.2 ± 0.1 nm, as measured by variable angle spectroscopic ellipsometry (VASE), corresponding to a grafting density (σ) of 0.27 chains nm^{-2}. *c*-PCPOXA brushes showed a slightly higher T_{dry} of 3.8 ± 0.1 nm, which indicated a higher polymer surface coverage with σ = 0.34 chains nm^{-2}. As was previously observed in the case of neutral PAOXA assemblies,[20, 21, 25, 47] the formation of denser polyacid grafts by adsorption of cyclic adsorbates is presumably due to their more compact molecular dimensions, compared to linear analogues of similar molar mass,[10, 11, 14] which reduced steric hindrance between surface-interacting polymers.

The formation of PCPOXA brushes was subsequently studied *in situ*, by monitoring the adsorption of *l*- and *c*-PCPOXA adsorbates with quartz crystal microbalance with dissipation (QCM-D), using Au-coated sensors as substrates. As shown in Figure 1a, the formation of both linear and cyclic brushes displayed distinctly rapid kinetics, as witnessed by a quick drop in the values of frequency (ΔF) just after injection of PCPOXA solutions in the QCM-D cells.

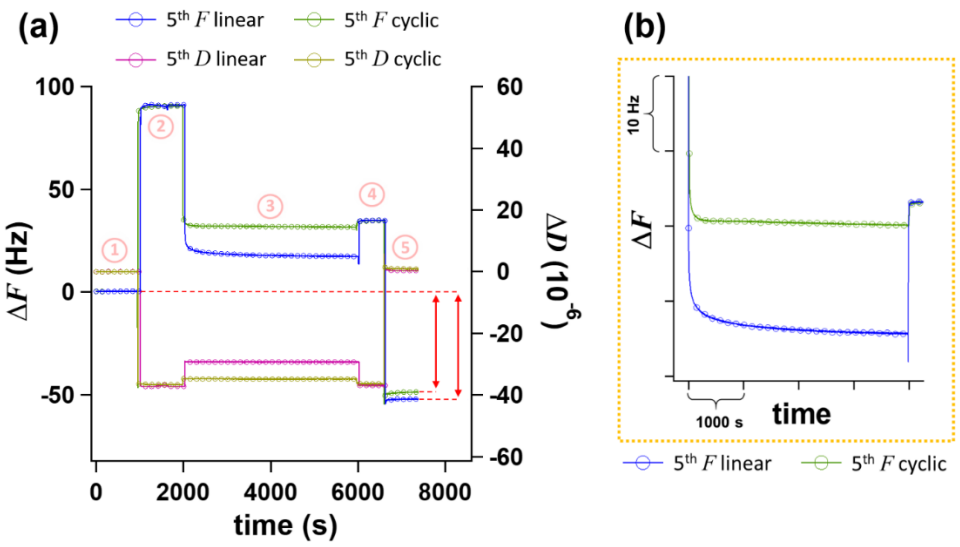

Figure 1. (a) Assembly of *l*- and *c*-PCPOXA on Au-coated sensors monitored by QCM-D recording ΔF and ΔD shifts, following (1) incubation in ultra-pure water, (2) methanol-1% acetic acid, (3) 1 mg ml^{-1} *l*- and *c*-PCPOXA solutions in methanol-1% acetic acid, (4) rinsing with methanol-1% acetic acid, and (5) final rinsing with ultra-pure water. One representative overtone (5^{th}) is shown for *l*-PCPOXA (5^{th} F linear and 5^{th} D linear, blue and violet traces), and for *c*-PCPOXA (5^{th} F cyclic and 5^{th} D cyclic, green and yellow traces). The red arrows highlight the final values of ΔF recorded in ultra-pure water for *l*- and *c*-PCPOXA brushes (differences between (1) and (5)). (b) A zoomed-in sensogram displaying the variation of ΔF during the adsorption of *l*-PCPOXA (blue trace) and *c*-PCPOXA (green trace) from 1 mg ml^{-1} methanol-1% acetic acid polymer solutions.

For both *l*- and *c*-PCPOXA brushes, the observed initial fast adsorption was followed by a plateau, suggesting surface saturation by adsorbing polymers (Figure 1b). However, in the case of cyclic brushes, ΔF reached a nearly constant value within a few minutes, while the assembly of *l*-PCPOXA was more gradual, with ΔF progressively approaching a steady-state value more than 30 min after injection. The assembly of *l*- and *c*-PCPOXA brushes was followed by washing the sensors with pure solvent, in order to remove any weakly adsorbed

polymer from the Au surfaces (point 4 in Figure 1a). During this process, slight but significant differences could also be observed by comparing the behavior of the just-formed linear and cyclic brushes.

In particular, a marked increment in ΔF, corresponding to a decrease in adsorbed mass on the sensor, accompanied the washing step on *l*-PCPOXA films, indicating that a relatively large amount of physisorbed/weakly attached chains had been present. In contrast, ΔF increased by just a few Hz while rinsing *c*-PCPOXA brushes, suggesting that a more stably grafted layer was formed.

Hence, the analysis of QCM-D results revealed that, although both linear and cyclic adsorbates rapidly adsorbed on Au, the more compact character of *c*-PCPOXA species favored a relatively quick surface saturation by polymer grafts, in a similar way as was previously described while comparing the assembly of dendron-like and linear poly(ethylene glycol)s (PEG) of similar molar mass.[48] *l*-PCPOXA adsorbates also underwent rapid assembly on Au, although this was accompanied by a significant physisorption of linear chains, which were presumably dangling at the formed brush interface.

Acquisition of ΔF and dissipation (ΔD) values in ultra-pure water (point 5, Figure 1a) finally enabled us to estimate the hydrated thickness (T_{wet}) of the assembled films (Supporting Information), which resulted 11.1 ± 0.3 and 9.4 ± 0.2 nm, for *l*- and *c*-PCPOXA brushes, respectively. The values of T_{wet} obtained by QCM-D could be correlated to the corresponding T_{dry} derived from VASE, finally yielding the swelling ratio of the assemblies ($SR = T_{wet}/T_{dry}$), which resulted 3.6 and 2.5, for linear and cyclic grafts, respectively.

The significantly lower value of SR recorded for *c*-PCPOXA was implicitly determined by the structure of cyclic brushes, which cannot vertically extend as much as linear grafts of comparable molar mass when immersed in a good solvent. This phenomenon confirms the distinctive compactness of *c*-PCPOXA brushes. On the one hand, cyclic grafts are

characterized by slightly higher values of σ, due to their less hindered surface-assembly process.[21] On the other hand, they feature an intrinsically higher polymer segment density in the hydrated state, due to the structural necessity of each polymer chain to loop down to the grafting point.[20]

Effect of Grafted-Polymer Topology on pH-Responsiveness

In order to systematically investigate how grafted-chain topology determined the responsive behavior of PCPOXA brushes, we alternately subjected linear and cyclic assemblies to aqueous solutions of different pH values, while recording their swelling properties, and nanomechanical/nanotribological characteristics by a combination of QCM-D and AFM-based methods.

Topologically different PCPOXA films were subjected to extremely diluted buffer solutions (1 mM acetic acid /sodium acetate buffer for pH 3.0, 4.5 and 6.3, and 1 mM phosphate buffer for pH 7.4, 8.5, 10.5, Supporting Information), in order to exclude the effect of ionic strength on the brush deprotonation-induced swelling.[49-51] As reported in Figure 2a, the values of ΔF for both *l*- and *c*-PCPOXA brushes showed a significant decrease at pH > 6, indicating that the deprotonation of polyacid grafts was accompanied by a marked increment in the hydrated mass of the films. Interestingly, a very similar, general trend was observed for the two different polymer topologies, for which a comparable pK_a value between 6 and 6.5 was identified.[52, 53]

A similar result was recently reported by Veige *et al.*,[54] who demonstrated that linear and cyclic polyphenols display nearly the same value of pK_a when dissolved in aqueous media. QCM-D was used to evaluate the pH-dependent hydration and swelling of *l*- and *c*-PCPOXA brushes, by recording and analyzing the variations of ΔF and ΔD at different pH values.

Despite the transition of linear and cyclic polyacid grafts occurred at a similar pH values, the responsive properties of the films demonstrated a significant dependence on the topology of the grafted polymers. In particular, the overall variation of ΔF across the entire pH range was clearly broader for *c*-PCPOXA than for *l*-PCPOXA (Figure 2a). This phenomenon was confirmed by alternately subjecting linear and cyclic grafts to buffer solutions of pH = 3 (well below the pK_a) and pH = 10.5 (well above the pK_a) (Figure 2d).

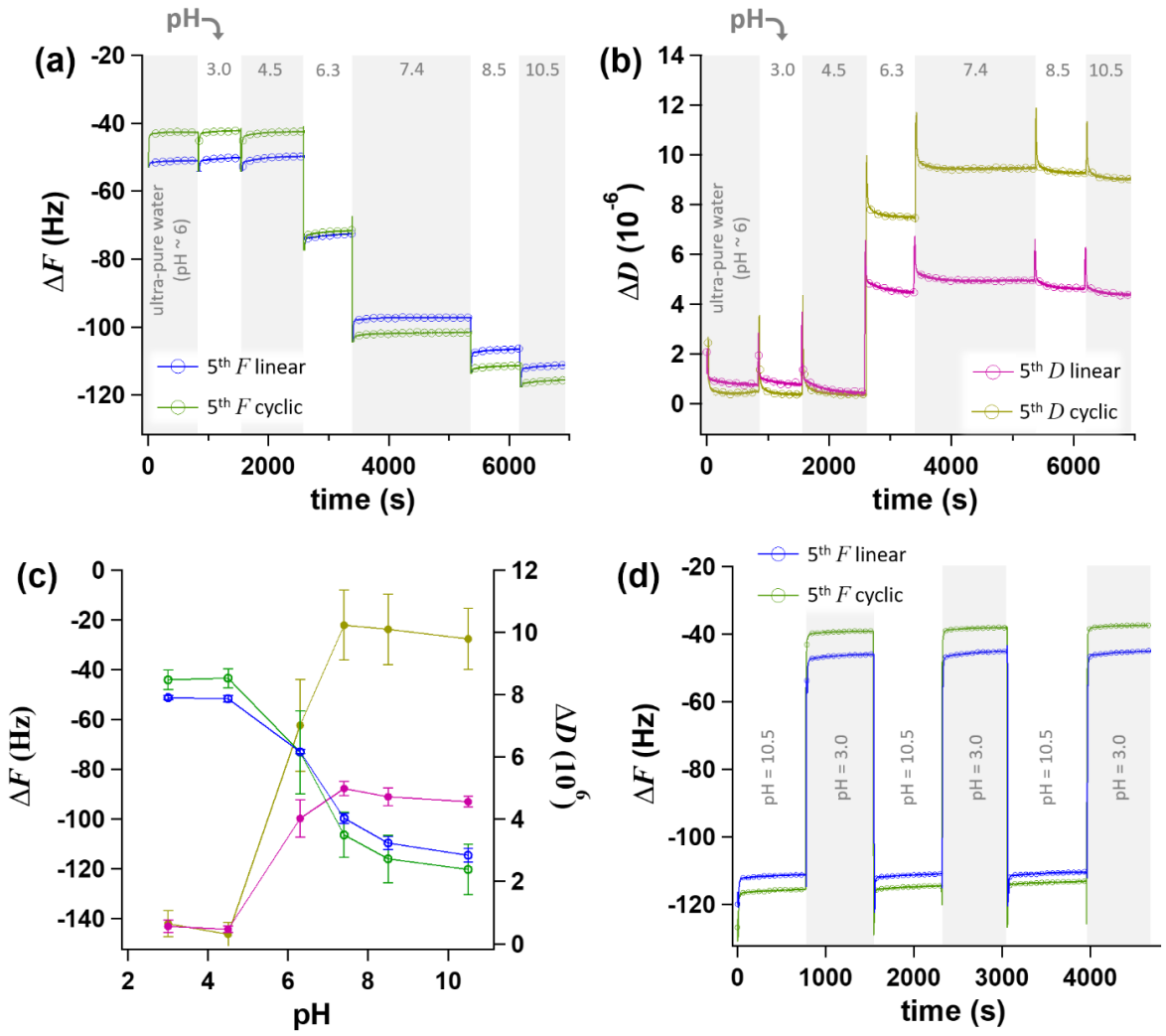

Figure 2. pH-responsive properties of *l*- and *c*-PCPOXA brushes studied by QCM-D. (a) Changes in ΔF recorded for *l*-PCPOXA (blue trace, 5th *F* linear) and *c*-PCPOXA (green trace, 5th *F* cyclic) during incubation in aqueous buffer solutions with different pH values. (b) Changes in ΔD recorded for *l*-PCPOXA (violet trace, 5th *D* linear) and *c*-PCPOXA (yellow

trace, 5th *D* cyclic) during incubation in aqueous buffer solutions with different pH values. (c) Absolute values of Δ*F* and Δ*D* as a function of pH for *l*-PCPOXA (blue and violet traces, for Δ*F* and Δ*D*, respectively), and *c*-PCPOXA brushes (green and yellow traces, for Δ*F* and Δ*D*, respectively). (d) Variation in Δ*F* recorded for *l*-PCPOXA (blue trace, 5th *F* linear) and *c*-PCPOXA (green trace, 5th *F* cyclic) during alternate incubations in aqueous buffer solutions of pH = 3.0 and 10.5.

The broader variation of Δ*F* with pH for cyclic brushes compared to their linear analogues corresponded to a larger shift in their swelling properties. As displayed in Figure 3a, T_{wet} of *c*-PCPOXA showed a relatively broad variation across the entire range of pH studied, progressively shifting from 9.0 ± 1.3 nm at pH 3, to 28.1 ± 0.7 nm at pH 10.5. In contrast, T_{wet} of *l*-PCPOXA varied to a lesser extent, increasing from 11.1 ± 0.9 nm at pH 3, to 26.2 ± 0.6 nm at pH 10.5.

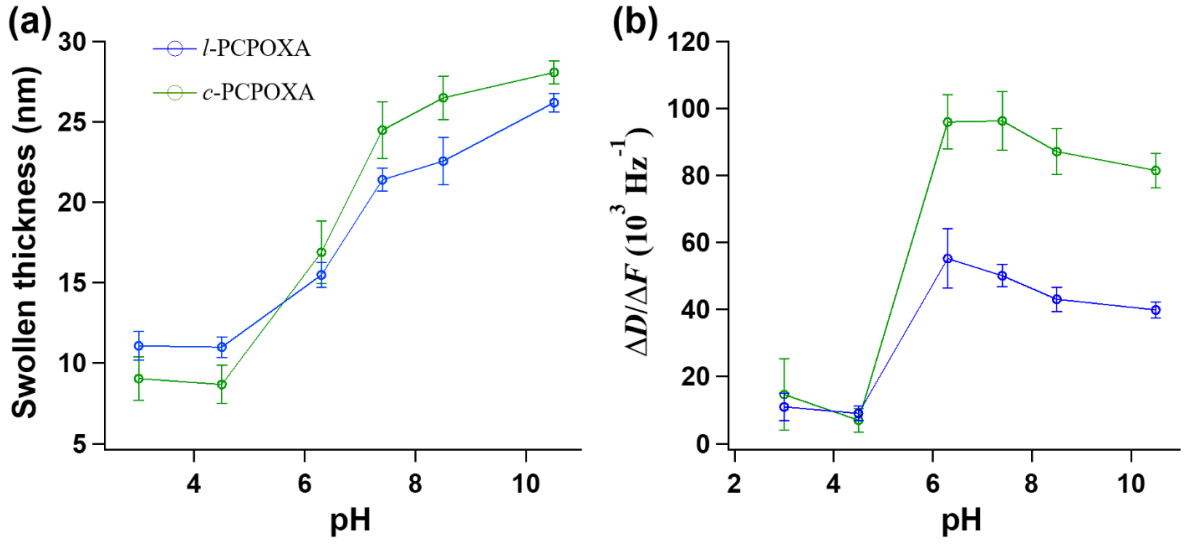

Figure 3. (a) Swollen thickness (T_{wet}) estimated from QCM-D for *l*-PCPOXA (blue trace) and *c*-PCPOXA brushes (green trace) by applying an extended viscoelastic model to Δ*F* and Δ*D* as a function of pH (Supporting Information). (b) The variation of Δ*D*/Δ*F* with pH

provides information about the change in viscoelastic properties accompanying a shift in hydrated mass of *l*-PCPOXA (blue trace) and *c*-PCPOXA brushes.

The observed, amplified pH-responsiveness of cyclic polyacid brushes was presumably due to their polymer architecture. Densely surface-grafted linear chains extend vertically toward the interface upon deprotonation, due to electrostatic repulsion between charged groups. Deprotonation of cyclic grafts, on the other hand, because of the intrinsic intramolecular steric constraints, leads to an enhanced electrostatic repulsion between charged polymer segments, and a concurrent, more marked expansion and swelling, compared to their linear counterparts (Scheme 1b). Hence, while *c*-PCPOXA brushes in their neutral state (pH < 6) show a lower vertical extension (and thus lower T_{wet}) with respect to linear analogues with nearly the same surface density and molar mass, upon charging (pH > 6) they experience an augmented electrostatic repulsion within their structure, which leads to a more pronounced expansion.

The higher level of hydration for charged cyclic brushes was also confirmed by analyzing how ΔD varies as a function of pH of the medium. As reported in Figures 2b and 2c, dissipation steadily increased above the pK_a for both *l*- and *c*-PCPOXA brushes. However, when pH > 6 the increment in ΔD recorded for cyclic grafts was twice as large as that observed for their linear analogues, suggesting a more significant hydration and degree of viscoelastic character in *c*-PCPOXA films at basic pH values.

Interestingly, for both *l*- and *c*-PCPOXA brushes the values of ΔD did not increase for pH > 7.4 (Figure 2b and 2c). In addition, the ratio between ΔD and ΔF, which provides an estimate of how the dissipative character of the films varies upon a corresponding variation in the amount of coupled solvent,[55] showed a progressive reduction above pH 7.4 (Figure 3b).

These data suggest that the observed increment in swelling by PCPOXA grafts was not accompanied by a simultaneous increase in viscoelasticity, probably due to electrostatic repulsive interactions within the brushes, which also lead to the formation of more rigid films.[56]

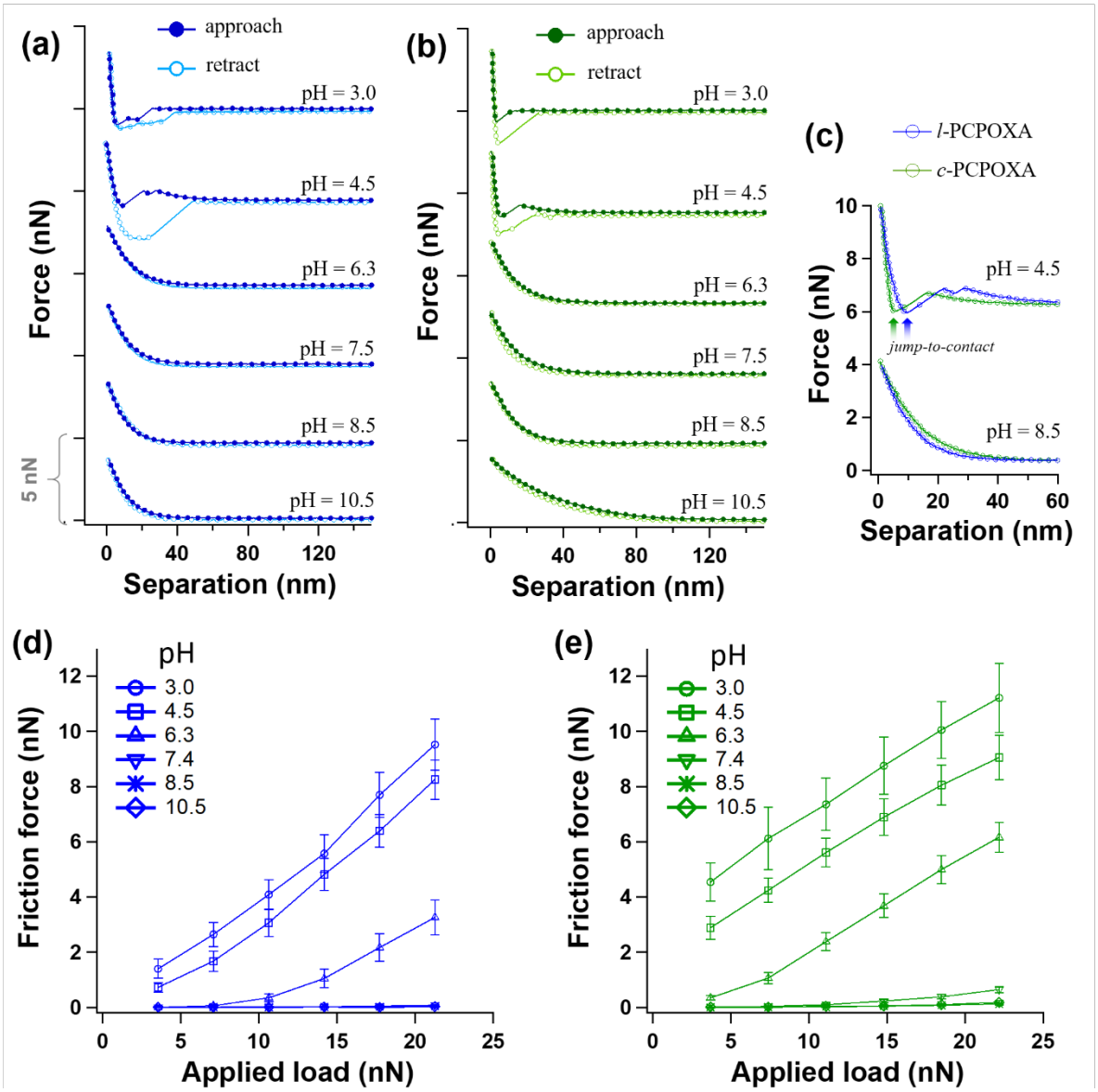

Figure 4. (a-c) Colloidal probe AFM was used to investigate the nanomechanical properties of *l*- and *c*-PCPOXA brushes. Topologically identical grafts were compressed while immersed in aqueous media of different pH values. Representative FS profiles are reported in (a) and (b), for linear and cyclic brushes, respectively. A scanning distance of 1 μm and a

scanning rate of 0.25 Hz was used to obtained the FS profiles. (c) Approaching FS curves recorded at pH = 4.5 and pH = 8.5 while compressing linear and cyclic PCPOXA brushes. The diameter of the Au-coated, silica colloidal probe was 20 μm, normal spring constant of the cantilevers, K_N = 0.096 N m^{-1} for both linear and cyclic PCPOXA brushes. (d-e) Friction force-*vs*-applied load (F_fL) profiles recorded by LFM while shearing topologically identical brush surfaces immersed in aqueous media presenting different pH, and alternatively functionalized with (d) *l*-PCPOXA and (e) *c*-PCPOXA brushes. A scanning distance of 2 μm and a scanning rate of 0.5 Hz was used for the friction measurements (Supporting Information).

The pH-responsive behavior of topologically different PCPOXA brushes could be also demonstrated by analyzing their nanomechanical and nanotribological properties by AFM. In particular, the interfacial, nanomechanical properties of *l*- and *c*-PCPOXA brushes were investigated by colloidal probe microscopy (CPM), by compressing the films with an Au-coated colloidal probe functionalized with an identical PCPOXA brush, while recording force-*vs*-separation curves (FS).[57]

As highlighted in Figures 4a and 4b, both linear and cyclic brushes at acidic pH values displayed adhesive interactions, with jump-to-contact events along the approaching profiles, followed by the occurrence of adhesive forces upon retraction. Under these conditions, the rather steep approach curves recorded beyond the contact point were likely due to the reduced swelling of linear and cyclic brushes, while adhesion upon retraction was generated by hydrogen bonding between protonated COOH groups on the opposing brushes.[58]

When pH was raised above the pK_a of the grafted polyacids, the highly swollen character of charged PCPOXA brushes, coupled with the electrostatic repulsive interactions between the opposing surfaces, dominated the FS profiles. On both brush types, the approach curves

showed repulsive behavior, although this was relatively more pronounced in the case of *c*-PCPOXA brushes, especially at high pH values. The amplified responsive behavior of cyclic grafts is highlighted when comparing the approach FS curves recorded on topologically different brushes below and above the pK_a (Figure 4c). At pH = 4.5, the FS curves recorded on cyclic brushes showed a steeper profile than that observed by compressing their linear counterparts, while the contact point between the opposing cyclic-brush surfaces was recorded at lower values of separation with respect to that observed by compressing linear analogues. These results agree well with the lower values of T_{wet} estimated by QCM-D on *c*-PCPOXA brushes, and their more compact morphology in the neutral state (acidic conditions). Conversely, at pH 8.5 a more pronounced repulsive behavior characterized the FS approach curves obtained on cyclic grafts, suggesting increased hydration with respect to their linear analogues. Overall, CPM analysis confirmed how *c*-PCPOXA films are more compact below, and more expanded above the pK_a, with respect to linear brushes (as depicted in Scheme 1b).

The more pronounced transition by cyclic polyacid brushes in response to a pH variation corresponds to a direct translation of topology effects typically observed in solution into surface properties, and it is determined by the intrinsically constrained configuration of cyclic grafts.

Lateral force microscopy (LFM) further illustrated how the variation in swelling and interfacial properties by *l*- and *c*-PCPOXA across the investigated pH range determined the friction between two opposed, topologically identical brushes shearing against one another. As displayed in the friction force-*vs*-applied load (F_fL) plots reported in Figures 4d and 4e, both linear and cyclic grafts showed high friction for pH < pK_a, with relatively high coefficients of friction (μ), which lay between 0.3 and 0.4. Friction significantly decreased around the pK_a (pH = 6.3), and reached extremely low values for pH ≥ 7.4, with μ dropping

to 10^{-3}-10^{-4} at pH = 10.5. Under these conditions, incorporation of water by linear and cyclic grafts provided a substantial increment in the amount of fluid lubricant, while increasingly repulsive electrostatic interactions between the sheared surfaces hindered collision between opposing polymer chains, and thus suppressed dissipation of mechanical energy.[59] Interestingly, no significant differences were observed when comparing the frictional properties of *l*- and *c*-PCPOXA brushes. Previous studies focusing on neutral, hydrophilic cyclic grafts have demonstrated that the absence of linear chain ends extending at the interface suppresses interdigitation between sliding brushes, and thus leads to extraordinary lubricity when compared to their linear counterparts. However, this effect could not be observed while analyzing the nanotribological properties of topologically different polyelectrolyte brushes, presumably due to partial charging of the films, especially at pH > pK_a, *i.e.* when these become "lubricious". Electrostatic repulsion significantly reduces interpenetration between opposing grafts, for both linear and cyclic brushes, and appears to be the principal parameter determining the suppression of dissipative forces between sliding surfaces, rather than grafted-chain topology.

Protein Binding by Linear and Cyclic Polymer Brushes

Having established how topology effects can substantially alter the responsive properties of surface-grafted-polymer assemblies, we subsequently investigated their application as functional platforms for the selective immobilization of proteins.

In particular, linear and cyclic PCPOXA adsorbates were first modified by coupling galactosamine to their COOH functions (Scheme 2a and 2b, and Supporting Information), yielding poly(2-N-2-deoxy-D-galactopyranosecarboxamidepropyl-2-oxazoline) (PGalaPOXA) with ~ 40 mol% of sugar moieties distributed along the polymer backbones (Supporting Information). Linear and cyclic PGalaPOXA (*l*-PGalaPOXA and *c*-PGalaPOXA,

respectively) were subsequently assembled on Au surfaces from 1 mg mL^{-1} aqueous solutions. Unexpectedly, the dry thickness of linear grafts was slightly higher than that recorded on cyclic analogues, as measured by VASE, namely T_{dry}(*l*-PGalaPOXA) = 3.7 ± 0.2 nm, while T_{dry}(*c*-PGalaPOXA) = 3.0 ± 0.1 nm, resulting in σ of 0.21 and 0.18 chains nm^{-2} for *l*-PGalaPOXA and *c*-PGalaPOXA, respectively. This was a rather surprising result, since, in common with other polymer types *c*-PGalaPOXA adsorbates show smaller hydrated dimensions with respect to their linear counterparts of comparable molar mass (Supporting Information), and thus should be sterically less hindered while assembling on surfaces, finally yielding denser and thicker films in the dry state. However, QCM-D confirmed the formation of slightly thicker *l*-PGalaPOXA brushes compared to *c*-PGalaPOXA films, although the assembly kinetics observed for linear and cyclic adsorbates showed similar behaviors (Supporting Information).

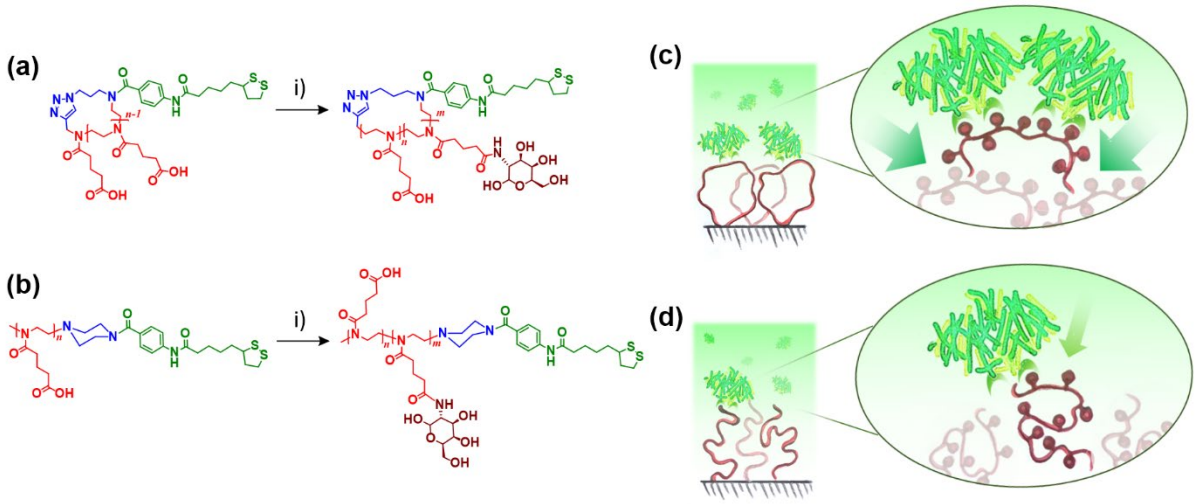

Scheme 2. Synthesis of *c*-PGalaPOXA (a) and *l*-PGalaPOXA (b) through modification of *l*-PCPOXA and *c*-PCPOXA, respectively. Conditions applied in (i): galactosamine hydrochloride, 1-ethyl-3-(3-(dimethylamino)propyl)carbodiimide hydrochloride (EDC-HCl), 2-morpholinoethanesulfonic acid hydrate (MES) buffer, pH = 4.7, 25°C, 24 h. (c,d) Schematic illustrations displaying the more efficient exposure of functional groups and the

consequent increased protein binding ability of cyclic brushes (c), compared to their linear counterparts (d).

Glycopolymers featuring multiple sugar functions have been demonstrated to strongly bind to lectins, due to the cluster glycoside effect.[44] In addition to binding-unit concentration,[60] the chain microstructure of multi-block copolymers[61-64] and controlled branching[65-69] are factors that determine the exposure of sugar moieties, and thus further influence the strength and kinetics of association with proteins. The effect of macromolecular topology on the reactivity of synthetic glycopolymers toward lectins however remains basically unexplored, especially in the case of surface-grafted polymer assemblies.

The specific binding of lectins to topologically different PGalaPOXA brushes was investigated by a combination of VASE and QCM-D. We specifically focused on the adsorption of Jacalin (0.1 mg mL^{-1} in phosphate buffer saline solution, PBS, with pH = 7.4), a relatively small protein that binds to human serum and secretory immunoglobulin A (sIgA), and which is reactive toward the Thomsen-Friedenreich antigen—a tumor-associated antigen that is linked to malignancy.[70]

Jacalin strongly bound to PGalaPOXA surfaces due to its high affinity toward galactose functions,[71] forming uniform protein layers with dry thickness ($T_{Jacalin}$) ≥ 5 nm (inset in Figure 5a). The attachment of proteins followed rapid kinetics, both on *l*-PGalaPOXA and *c*-PGalaPOXA brushes, as monitored by QCM-D (Figure 5b), although both VASE and QCM-D showed a significantly higher amount of proteins adsorbing on cyclic grafts. Namely, $T_{Jacalin}$ was 4.9 ± 0.2 and 6.0 ± 0.1 on linear and cyclic brushes, respectively ($p < 0.001$, inset in Figure 5a), while the hydrated mass of proteins ($m_{Jacalin}$) extracted from ΔF values of QCM-D data indicated 913 ± 40 and 1330 ± 25 ng cm^{-2} bound to *l*-PGalaPOXA and *c*-PGalaPOXA, respectively (Supporting Information).

Since VASE data can be directly translated into dry mass of adsorbed proteins, by considering the surface coverage of linear and cyclic brushes, we could estimate the relative binding capacity of each graft type, which resulted 0.29 and 0.42 proteins chain^{-1} ($p < 0.05$) for *l*-PGalaPOXA and *c*-PGalaPOXA, respectively (Figure 5a).

Hence, a nearly 45% increment in protein binding was achieved by substituting linear brushes for their cyclic analogues that featured a similar content of galactose units, and this result was confirmed both by QCM-D and VASE.

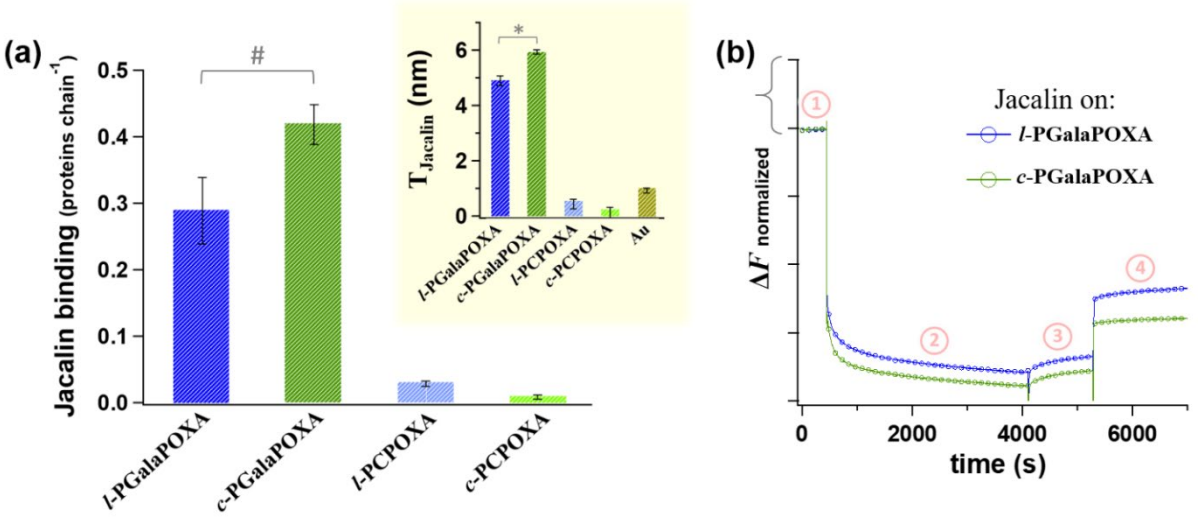

Figure 5. (a) Jacalin binding per polymer graft (expresses as no. of proteins chain^{-1}) obtained from VASE data for *l*-PGalaPOXA and *c*-PGalaPOXA brushes. Binding of Jacalin on *l*-PCPOXA and *c*-PCPOXA was measured as control. In the inset, the dry thickness by VASE of Jacalin layer formed on *l*-PGalaPOXA and *c*-PGalaPOXA brushes was reported. The corresponding *l*-PCPOXA and *c*-PCPOXA were applied as controls, together with bare Au surfaces. (b) Variation of ΔF recorded with QCM-D on Au sensors coated with *l*-PGalaPOXA (blue trace) and *c*-PGalaPOXA brushes (green trace), and subjected to 0.1 mg mL^{-1} PBS solution of Jacalin. Brush-coated Au sensors were first flushed with PBS (1), followed by 1 h incubation in Jacalin solution (2), rinsing with PBS (3) and final washing

with ultra-pure water (4). * and # indicate statistically significant differences between the set of data (* $p < 0.001$; # $p < 0.05$).

Although a slightly lower polymer surface crowding (-17%) could favour a more pronounced protein association to cyclic brushes with respect to that observed on their denser, linear counterparts, the significantly augmented affinity of Jacalin toward *c*-PGalaPOXA brushes (+45%) was likely a direct effect of polymer topology. In particular, due to the intramolecular steric constraints generated within cyclic glycopolymers, functional groups are more exposed when compared to those on linear-brush analogues. As galactose moieties along a cyclic graft tend to interact more favorably with their surrounding rather than coiling or associating with neighboring functions,[27] they are more accessible to the galactose-binding pockets of Jacalin. Similarly, functional glycopolymers capable of forming folded, "loop"-like segments through supramolecular junctions have recently been shown to increase the exposure of sugar moieties in solution, interacting more efficiently with different proteins.[72]

On surfaces, the distinctive configuration of cyclic polymer brushes, where functional chains extend from the grafting surface and loop back to their anchor, enables an enhancement of multivalent binding interactions with lectins.

CONCLUSIONS

The translation of the topology effects in functional, cyclic polymer adsorbates into surface properties of brush assemblies leads to an amplification of their responsive properties and an enhancement in their bioreactivity. The distinctive architecture of cyclic polyacid brushes limits their swelling properties below the pK_a, while the steric tension intrinsic in their constrained topology triggers an augmented expansion and increased hydration upon deprotonation, when compared to their linear counterparts. The amplified pH-responsiveness

of cyclic polyelectrolyte brushes thus enables the tuning potential for interfacial physicochemical and nanomechanical properties on surfaces to be broadened, enabling the future application of topological polymer chemistry in the design and functionalization of "smart" materials.

When polyacid adsorbates were partially derivatised with galactose functions, the subsequently generated assemblies showed a topology-dependent affinity toward sugar-binding proteins. In particular, concentrating on the interaction with Jacalin—a tumor-specific lectin—the expanded structure of cyclic grafts provides an augmented exposure of galactose functions toward surface-approaching proteins, leading to ~ 45% higher Jacalin-binding capacity per polymer graft with respect to sugar-decorated linear analogues of comparable composition and molar mass.

The increased availability of ligands for lectins on cyclic grafts suggests that a topology-dependent enhancement in reactivity towards biological entities can be generalized to different types of substrates, and diverse polymer chemistries. While the validation of this hypothesis is currently being carried out in our laboratories, the application of cyclic polymers as synthetic supports for biological recognition can be realistically envisioned as a tool for improving the performance of nanomedical devices and biosensors.

METHODS

Materials

Glutaric anhydride (95%), methyl *p*-toluenesulfonate (MeOTs, 98%), (2-chloroethyl)trimethylammonium chloride (99%), 4-(dimethylamino)pyridine (DMAP, 99%), 3-bromopropylammonium bromide (98%), piperazine (≥99.0%), magnesium sulfate ($MgSO_4$, anhydrous, ≥99.5%), sodium carbonate (Na_2CO_3, anhydrous, ≥99.5%) potassium hydroxide (KOH, ≥98.5%), lithium bromide (LiBr, >99%), sodium phosphate dibasic dihydrate

(Na_2HPO_4, 99%), calcium hydride (CaH_2, 95%), sodium azide (NaN_3, ≥99.5%), sodium methoxide (NaOMe, 95%), thionyl chloride ($SOCl_2$, ≥99%), trifluoroacetic acid (TFA, ≥99.0%), hydrochloric acid (HCl, >37%), N,N-diisopropylethylamine (DIPEA, 99.5%), acetonitrile (ACN, 99.9+% HPLC grade), methanol (MeOH, >99.9% HPLC grade), N,N-dimethylformamide (DMF, >99%), diethyl ether (Et_2O, ≥99.8), ethyl acetate (EtOAc, 99.8+%), acetic acid (AcOH, >99.8%), copper(I) bromide (CuBr, 99.999% trace metals basis), barium oxide (BaO, ≥99.5%) were purchased from Sigma Aldrich. 1-Hydroxy-7-azabenzotriazole (HOAt, >98%) was purchased from TCI chemicals. Ethanol (EtOH, ≥99.8%), toluene (≥99.5%), sodium hydroxide (NaOH, ≥98.5%), and ammonium chloride (NH_4Cl, 99.5%) were purchased form VWR Chemicals. Propargyl *p*-toluenesulfonate (propargyl tosylate, 97%), triethylamine (TEA, 99%), dichloromethane (DCM, 99.8% extra dry over MS), DCM (>99% extra pure+Amylene), ACN (99.8%, extra dry over MS), MeOH (99.8%, extra dry over MS), DMF (99.8%, extra dry over MS), (±)-α-Lipoic acid (>98%), N,N,N',N'',N''-pentamethyldiethylenetriamine (PMDETA, >99%) were purchased from Acros Organics. 2-morpholinoethanesulfonic acid hydrate (MES hydrate), 1-ethyl-3-(3-(dimethylamino)propyl)carbodiimide hydrochloride (EDC HCl), galactosamine hydrochloride, (1-cyano-2-ethoxy-2-oxoethylideneaminooxy)dimethylaminomorpholinocarbenium hexafluorophosphate (COMU, 99%) were purchased form Fluorochem. Deuterium oxide (D_2O, 100%), chloroform-d ($CDCl_3$, 99.8%) and dimethyl sulfoxide-d6 (DMSO-d_6, 99.8%) were purchased from Cambridge Isotope Laboratories. TEA was distilled over KOH prior to use, and stored under argon. MeOTs and propargyl tosylate were distilled under high vacuum over CaH_2, and stored under argon. CuBr was purified by stirring in AcOH overnight, followed by washing with copious amounts of MeOH and Et_2O, vacuum filtration and drying under high vacuum for 24 h. All the other chemicals were used as received.

Surface Assembly of PCPOXA and PGalaPOXA adsorbates on Au

Silicon wafers presenting 100 nm-thick Au layer were prepared by reactive magnetron sputtering (Paul Scherrer Institute, Villigen, Switzerland). The substrates (10 x 20 mm^2) were cleaned for 1 min in *Piranha* solution (3:1 mixture of concentrated H_2SO_4 and H_2O_2), and later on extensively washed with ultra-pure water and absolute ethanol. Surface assembly of *l*-PCPOXA and *c*-PCPOXA was performed by immersing Au-coated substrates for 2 h in 1 mg mL^{-1} polymer solutions in MeOH + 1% AcOH at room temperature (RT). The functionalized samples were subsequently rinsed with ultra-pure water and absolute ethanol to remove physisorbed species, and finally dried under a stream of N_2. Surface assembly of *l*-PGalaPOXA and *c*-PGalaPOXA was performed following a similar protocol, but using 1 mg mL^{-1} polymer solutions in ultra-pure water. All solutions were filtered over 0.2 μm filters (Spartan 13/0.2 RC, Whatman) prior to surface grafting.

Lectin Binding on PGalaPOXA Brushes

l-PGalaPOXA and *c*-PGalaPOXA-coated substrates were immersed in water for 1 h for rehydration, and then incubated in 0.1 mg mL^{-1} Jacalin solutions (Sigma-Aldrich®, USA) in PBS for 1 h, in a 24-well tissue culture plate (TPP®, Switzerland). Following incubation in protein solutions, the samples were rinsed with PBS and ultra-pure water, dried under N_2 and finally analyzed by VASE. Bare Au-coated wafers and PCPOXA-functionalized substrates were used as positive and negative controls, respectively.

Variable Angle Spectroscopic Ellipsometry (VASE)

The values of dry thickness (T_{dry}) of PCPOXA, PGalaPOXA and protein layers were measured with a variable-angle spectroscopic ellipsometer (M-2000F, Woollam Co., Inc., Lincoln, NE, USA). The measurements were performed in the spectral range of 290 – 900 nm using focusing lenses at three different angles of incidence from the surface normal (60°, 63°, and 69°). Each

data point resulted from an average of 20 measurements, and the obtained raw ellipsometric data were fitted with a bilayer model (Au and organic layer) using the analysis software WVASE32. The optical constants of the Au substrate (*n* and *k*) were experimentally obtained by analyzing a freshly cleaned, sputtered Au layer with known thickness. The organic layers (polymer brushes and/or protein films) were fitted using a Cauchy model $n = A + B\,\lambda^{-2}$, where *n* is the refractive index, λ is the wavelength and A and B were assumed to be 1.45 and 0.01, respectively, as values for transparent organic films.[73] The values of T_{dry} for the polymer-brush layers were used to calculate the grafting density (σ), by applying the equation; $\sigma = \rho\, T_{dry}\, N_A\, M_n^{-1}$, where ρ is the density of the dry polymer, N_A is the Avogadro number, and M_n is the number average molecular weight of the adsorbate. A homogeneous mass distribution of the organic layer perpendicular to the Au surface was assumed, with a constant density (ρ) of 1.14 g cm^{-3} for PCPOXA and PGalaPOXA brushes and 1.35 g cm^{-3} for Jacalin.[74]

For all VASE experiments, mean values and standard deviations were calculated using three replicates per sample and measuring six points on each of them. Statistical significance was assessed by one-way ANOVA and Tukey's multiple comparison *post-hoc* test.

Quartz Crystal Microbalance with Dissipation (QCM-D)

The assembly of linear and cyclic adsorbates on Au surfaces, their pH-responsive properties and interaction with proteins were monitored *in situ* by QCM-D, using an E4 instrument (Q-Sense AB, Göteborg, Sweden) equipped with dedicated Q-Sense AB software. Au-coated crystals (LOT-Oriel AG) with a fundamental resonance frequency of 5 MHz were used as substrates. Before the experiment, the substrates were cleaned by sonication in toluene and 2-propanol, and UV-ozone treatment. After cleaning, the crystals were dried under a stream of N_2 and immediately used. The values of hydrated thickness (T_{wet}) of topologically different PCPOXA and PGalaPOXA brushes were obtained by applying an extended viscoelastic

model,[75] fitting the frequency (ΔF) and dissipation shifts (ΔD), by using three different overtones (5rd, 7th and 9th) for each sample. Four crystals for each film were used to calculate the mean values of T_{wet} and their standard deviations. The input parameters for the fitting were fluid density (997 Kg m^{-3}), layer density (1100 Kg m^{-3}) and fluid viscosity (0.009 kg m^{-1} s^{-1}). The following parameters were fitted whilst constrained to physically meaningful boundaries: layer viscosity (0.009 – 0.05 kg m^{-1} s^{-1}), layer shear thickness (10^4 - 10^8 Pa), and layer thickness (10^{-9} – 2 10^{-8} m).

The values of hydrated mass of Jacalin adsorbed on PGalaPOXA layers were obtained by applying a similar fitting procedure.

Atomic force microscopy (AFM)

Normal and lateral force measurements were carried out using a MFP3D AFM (Asylum Research, Oxford Instruments, Santa Barbara, USA). Experiments were performed in a liquid cell filled with buffered solutions presenting different pH. Two tipless cantilevers (HQ:CSC38-C/tipless/Cr-Au, Mikromasch, Bulgaria) were chosen from the same box, and their normal (K_N) and torsional (K_T) spring constants were measured by applying the thermal noise[2] and Sader's method,[76] respectively (Table S1). Later on, silica microparticles (EKA chemicals AB, Kromasil R, Sweden) with a diameter of ~ 20 μm were glued onto the end of the calibrated cantilevers by using a two-component epoxy glue, using a custom-made micromanipulator. In order to functionalize the prepared colloidal probes with PCPOXA adsorbates, 3 nm-thick W and 20 nm-thick Au layers were deposited by using a metal evaporator (MED020 coating system, BAL-TEC, Balzers, Lichtenstein). *l*-PCPOXA and *c*-PCPOXA brushes were later on grafted following the same procedures applied for the flat Au-coated substrates.

Friction force measurements were carried out by acquiring 5-6 'friction loops' along the same line for each applied load over 3 different positions on each substrate. From this set of measurements average values and standard deviations of friction forces were calculated. A

scanning distance of 2 μm and a scanning rate of 0.5 Hz was used during the measurements. Lateral force calibration was performed using the method described by Cannara *et al.*.[77]

In order to estimate the adhesion properties of the different brush surfaces 40 force-*vs*-separation (FS) curves were recorded over 3 different positions for each substrate. A scanning distance of 1 μm and a scanning rate of 0.25 Hz was used to record each FS curve.

Force maps were recorded over an area of 20x20 μm^2 at three different positions for each sample (Figure S1a). Each force map consisted of 40 deflection-*vs*-Zsensor curves (Figure S1b). Later on, deflection-*vs*-Zsensor curves were analyzed by using the Asylum research AR13 software. Deflection was converted into force, while Zsensor was converted into separation by measuring the deflection sensitivity and K_N for the particular cantilever used (Figure S1c).

We assumed separation = zero as the point where the AFM colloidal probe fully compressed the two opposing brushes and was sensing the underlying substrate (*i.e.* hard-wall repulsion). At this point, the slope of a force-*vs*-separation profile was maximum and became constant (Figure S1d).

Brush-to-brush contact could be estimated for *l* and *c*-PCPOXA brushes immersed in aqueous media at acidic pH. Under these conditions, the FS profiles showed jump-to-contact events (Figure 4c), which could be directly correlated to the vertical separation at which the two opposing brushes come into contact (also corresponding to the swollen thickness).

NMR Spectroscopy

^{1}H- and ^{13}C-NMR spectra were recorded on a Bruker Avance III HD 400 MHz and a Bruker Neo 500 MHz spectrometer at RT using D_2O, $CDCl_3$, or DMSO-d_6 as solvents.

Size Exclusion Chromatography (SEC)

SEC of the precursor PMCPOXA species was performed at 45 °C with a Malvern VISCOTEK SEC_{max} VE-2001 instrument, equipped with two D5000 columns (300 × 8.0 mm) in series, refractive index (RI), viscometry, and light scattering (15° and 90° angles) detectors. The eluent used was DMF containing LiBr (1 g L^{-1}), at a flow rate of 1 mL min^{-1}. The values of M_n, M_w, and dispersity ($Đ$) of the synthesized polymers were determined by conventional calibration with poly(methyl methacrylate) (PMMA) standards using Malvern's OmniSEC software.

Aqueous SEC analysis of *l*- and *c*-PGalaPOXA was performed on an Agilent 1260 Infinity II HPLC system equipped with a refractive index detector over a PL aquagel-OH 20 (300 x 7.5 mm, 5 um) column. A mixture of H_2O:MeOH 7:3 (v/v) + 0.1 M LiBr was used as the eluent at 40 °C with a flow rate of 0.8 mL min^{-1}, calibrated using PEG standards.

Fourier-Transform Infrared Spectroscopy (FT-IR)

FT-IR spectra were recorded under vacuum using an infrared spectrometer (IFS 66 V, Bruker Optik GmbH, Germany) equipped with DTGS detector in transmission mode, in the 400-4000 cm^{-1} range at a resolution of 2 cm^{-1} and collecting 64 scans for each sample. The samples were measured as KBr pellets at a concentration of 2 mg g^{-1}.

The FT-IR spectrum of 3-azidopropylamine was recorded using a Bruker ALPHA FT-IR spectrometer in ATR (Ge crystal) mode in the 400-4000 cm^{-1} range at a resolution of 2 cm^{-1} and recording 64 scans.

Preparative Reverse-Phase High-Performance Liquid Chromatography (RP-HPLC)

Preparative RP-HPLC was performed on an Agilent Infinity 1260 prep-HPLC system with an Agilent C18 preparative HPLC column (50 x 150 mm, 10 μm) at a flow rate of 80 mL min^{-1} at RT using H_2O:ACN with 0.1% TFA as eluent.

Synthesis of (Ethyl 4-(5-(1,2-dithiolan-3-yl)pentanamido)benzoate) (BCLE, Figure S2, *step i*)

To a stirred solution of (±)-α-lipoic acid (2.0 g, 9.8 mmol, 1 eq.) in dry DCM (25 mL) were added HOAt (0.6 g, 4.4 mmol, 0.5 eq.) and DMAP (1.4 g, 30.0 mmol, 3 eq.) at RT and under inert atmosphere. After 30 minutes, benzocaine (1.6 g, 9.8 mmol, 1 eq.) was dissolved in dry DCM (5 mL) and added to the reaction solution. The reaction was monitored by using thin layer chromatography (TLC) (95/5 DCM:EtOAc). After 20 h, the reaction solution was diluted with DCM (150 mL) and the organic phase extracted with 1M HCl solution (2 x 100 mL), followed by 10% aqueous $NaHCO_3$ (100 mL), brine (100 mL) and finally dried using anhydrous $MgSO_4$. Removal of DCM provided the crude compound, which was purified by silica gel (SiliaFlash® P60 40-63µm) flash column chromatography using 95/5 DCM:EtOAc as eluent. The obtained compound was further purified by C18 preparative HPLC using a gradient from 50 to 100% ACN in water with 0.1% TFA as eluent. BCLE was obtained as a light yellow oil in moderate yield (2.4 g, 6.8 mmol, 70%). HPLC-MS-SQ [M+H]+ (355 m/z). ^{1}H-NMR (500 MHz, $CDCl_3$) δ = 9.08 (b, 1H), 8.04 – 7.89 (m, 2H), 7.69 – 7.56 (m, 2H), 4.34 (dq, J = 20.5, 7.1 Hz, 2H), 3.56 (dq, *J* = 8.7, 6.3 Hz, 1H), 3.22 – 3.06 (m, 1H), 2.70 (s, 3H), 2.51 – 2.37 (m, 2H), 1.96 – 1.62 (m, 4H), 1.59 – 1.45 (m, 2H), 1.37 (dt, *J* = 18.4, 7.1 Hz, 4H) ppm; ^{13}C-NMR (126 MHz, $CDCl_3$) δ = 171.8, 166.3, 142.3, 130.7, 127.9, 118.9, 60.9, 56.4, 40.2, 38.5, 37.4, 34.6, 28.8, 25.1, 14.4 ppm. (Figure S7).

Synthesis of (4-(5-(1,2-dithiolan-3-yl)pentanamido)benzoic acid) (BCLA, Figure S2, *step ii*)

12 mL of 1 M NaOH solution (480 mg, 12.0 mmol, 2 eq.) were added to a solution of BCLE (2.1 g, 5.9 mmol, 1 eq.) in 40 mL EtOH and 30 mL H_2O, and the mixture was heated to reflux. After 3 h (TLC showed quantitative hydrolysis of the ethyl ester), the reaction solution was

cooled down to RT, and 15 mL of 1 M HCl were added dropwise while a precipitate formed. Later on, the solution was poured in 200 mL of a stirred solution of water and ice, the precipitate was collected by vacuum filtration and washed with additional 200 mL of water. The solid was dried under high vacuum yielding a light yellow powder (1.75 g, 5.4 mmol, 90.5%).

^{1}H-NMR (500 MHz, DMSO-d_6) δ = 12.67 (s, 1H), 10.18 (s, 1H), 7.91 – 7.81 (m, 2H), 7.73 – 7.64 (m, 2H), 3.63 (dq, J = 8.7, 6.2 Hz, 1H), 3.18 (ddd, J = 11.0, 6.9, 5.5 Hz, 1H), 3.11 (dt, J = 11.0, 6.8 Hz, 1H), 2.47 – 2.36 (m, 1H), 2.35 (t, J = 7.4 Hz, 2H), 1.88 (dp, J = 12.8, 7.0 Hz, 1H), 1.76 – 1.52 (m, 4H), 1.48 – 1.34 (m, 2H) ppm; ^{13}C NMR (126 MHz, DMSO-d_6) δ = 171.7, 166.9, 143.3, 130.4, 124.9, 118.2, 56.1, 39.9, 38.1, 36.3, 34.2, 28.3, 24.8 ppm. (Figures S8 and S9).

Synthesis of 3-Azidopropylamine (Figure S3)

3-Bromopropylamine hydrobromide (14.0 g, 64.0 mmol, 1 eq.) was dissolved in 100 mL water. NaN_3 (13.7 g, 211.0 mmol, 3.3 eq.) was added to the solution, and the mixture was heated to reflux and stirred for 24 h. Upon completion of the reaction, half of the water was evaporated under vacuum, and the remaining solution was cooled down using an ice/water bath. The pH of the solution was raised to 14 by slowly adding KOH pellets while keeping the temperature below 10 °C. Subsequently, Et_2O (200 mL) was added. The organic layer was separated and the aqueous phase was extracted with Et_2O (2 x 100 mL). The combined organic phases were dried with $MgSO_4$ and filtered, and the solvent was carefully removed under vacuum yielding the crude compound as an off white oil (6.0 g, 59.9 mmol, 93.7%). The compound was stored at -20°C in the dark, and used without further purification for the termination of CROP.

^{1}H-NMR (500 MHz, $CDCl_3$) δ = 3.36 (t, J = 6.7 Hz, 2H), 2.79 (t, J = 6.8 Hz, 2H), 1.71 (p, J = 6.8 Hz, 2H) ppm; ^{13}C-NMR (126 MHz, $CDCl_3$) δ 49.1, 39.3, 32.4 ppm. ATR-FTIR (thin, cm-1): 2925, 2105, 1631, 1398, 1117, 618. (Figures S10 and S11).

Synthesis of methyl 5-chloro-5-oxopentanoate (Figure S4, step i)

A catalytic amount of NaOMe (474 mg, 8.8 mmol, 0.02 eq.) was added to a solution of glutaric anhydride (50.0 g, 438.2 mmol, 1 eq.) in dry MeOH (200 mL), and the mixture was heated to reflux for 6 h. After solvent removal under vacuum 5-methoxy-5-oxopentanoic acid (64.0 g, 437.9 mmol, 99.9%) was obtained, and used without further purification.

^{1}H-NMR (400 MHz, $CDCl_3$): δ = 3.67 (s, 3H), 2.46 (t, J = 7.5 Hz, 2H), 2.40 (t, J = 7.5 Hz, 2H), 1.96 (m, J = 7.5 Hz, 2H) ppm; ^{13}C-NMR (100 MHz, $CDCl_3$): δ = 179.1, 173.6, 51.5, 32.8, 32.7, 19.6 ppm.

$SOCl_2$ (38 mL, 525.5 mmol, 1.2 eq.) and few drops of dry DMF (cat.) were added to a solution of 5-methoxy-5-oxopentanoic acid (64.0 g, 437.9 mmol, 1 eq.) in DCM (200 mL), and the mixture was heated to reflux for 7 h until the formation of gases ceased. The solvent was removed under reduced pressure, and the excess $SOCl_2$ was co-evaporated with 50 mL of toluene. The resulting brownish residue was purified by fractional distillation (110°C, 40 mbar), yielding a colorless oil (64.6 g, 392.3 mmol, 89.6%).

^{1}H-NMR (400 MHz, $CDCl_3$): δ = 3.68 (s, 3H), 2.99 (t, J = 7.0 Hz, 2H), 2.40 (t, J = 7.0 Hz, 2H), 2.09-1.95 (m, 2H) ppm; ^{13}C-NMR (100 MHz, $CDCl_3$): δ = 173.0, 172.5, 52.10, 41.8, 33.4, 22.0 ppm.

Synthesis of methyl 5-((2-chloroethyl)amino)-5-oxopentanoate[78] (Figure S4, step ii)

Methyl 5-chloro-5-oxopentanoate (50.0 g, 303.8 mmol, 1 eq.) and 2-chloroethylammonium chloride (37.0 g, 319.0 mmol, 1.05 eq.) were suspended in dry DCM (400 mL) under N_2, and cooled down to 0 °C with an ice bath. TEA (53 mL, 380.0 mmol, 2.2 eq.) was added dropwise to the mixture over a period of 2 h. The suspension was warmed up to RT, and stirred overnight under an argon atmosphere. Later on, water (100 mL) was added and two phases separated.

The organic phase was washed with 1 M HCl, water (2x) and brine (each 100 mL), and finally dried over anhydrous $MgSO_4$. After filtration and solvent removal, the residual yellow oil was distilled under high vacuum (bp. 122°C, 4.8 x 10^{-2} mbar) to yield a light yellow oil (54.6 g, 262.9 mmol, 86.5%).

^{1}H-NMR (500 MHz, $CDCl_3$): δ = 6.33 (s, 1H), 3.65 (s, 3H), 3.61 – 3.49 (m, 4H), 2.64 (t, J = 6.8 Hz, 2H), 2.49 (t, J = 6.7 Hz, 2H) ppm; ^{13}C-NMR (126 MHz, CDCl3) δ = 173.45, 171.78, 51.94, 43.91, 41.36, 30.89, 29.30 ppm. (Figures S12 and S13).

Synthesis of 2-methoxycarbonylpropyl-2-oxazoline[5] (MCPOXA, Figure S4, step iii)

Methyl 5-((2-chloroethyl)amino)-5-oxopentanoate (54.6 g, 262.9 mmol, 1 eq.) and anhydrous Na_2CO_3 (25.1 g, 236.6 mmol, 0.9 eq.) were reacted in a 500 mL round-bottom flask mounted on a rotary evaporator (60°C, 50 mbar, 150 rpm) for 16 h, until the formation of CO_2 ceased. Later on, 200 mL of DCM were added, and the mixture was washed with 50 mL of brine. The two phases were separated, the organic phase was dried over $MgSO_4$, and the solvent was removed under reduced pressure. The crude product was obtained as a yellow oil, which was purified by distillation from BaO under high vacuum (bp. 81°C, 6.1 x 10^{-2} mbar), finally yielding a colorless oil (30.0 g, 175.2 mmol, 66.7%).

^{1}H-NMR (500 MHz, $CDCl_3$): δ = 4.3 (t, 9.5 Hz, 2H), 3.8 (t, 9.5 Hz, 2H), 3.7 (s, 3H), 2.7 (t, 7.3 Hz, 2H), 2.6 (t, 7.3 Hz, 2H), 1.97 (quint, 7.3 Hz, 2H) ppm; ^{13}C-NMR (126 MHz, $CDCl_3$) δ = 173.6, 167.8, 67.3, 54.5, 51.7, 32.9, 27.2, 21.3 ppm. (Figures S14 and S15).

Synthesis of PMCPOXA (Figure S5, step i)

To an oven-dried 50 mL Schlenk flask dry ACN (7 mL) and MCPOXA (3.51 g, 20.5 mmol, 50 eq.) were added under N_2. Later on, MeOTs (76.4 mg, 0.4 mmol, 1 eq.) was added at RT under N_2, and stirred for 10 min. The polymerization mixture was subsequently heated to 80 °C, and stirred for 16 h under argon. After this time, polymerization was cooled down to RT

and terminated by adding an excess of piperazine (706 mg, 8.2 mmol, 20 eq.) in 5 mL of dry DMF. The mixture was left stirring for additional 48 h under argon. The solvent was subsequently removed under reduced pressure, and the crude polymer was precipitated three times from DCM in Et_2O. The polymer was later on re-dissolved in H_2O:EtOH 1:1, and dialyzed in the same solvent using membranes with a molecular weight cut-off (MWCO) for 2 days at 4°C. After this time, EtOH was evaporated and the polymer was freeze-dried to yield PMCPOXA (3.1 g, 88% yield) as a white sticky polymer. The chemical structure and the purity of the synthesized polymer were determined by ^{1}H-NMR (500 MHz) (Figure S16). SEC analysis provided M_n = 8200, M_w = 10100 and $Đ$ = 1.23 (Figure S25).

Synthesis of l-PMCPOXA-BCLA (Figure S5, step ii)

PMCPOXA (550 mg, 0.06 mmol of secondary amine groups, 1 eq.), BCLA (100 mg, 0.3 mmol. 5 eq.) and COMU (140 mg, 0.33 mmol, 5.5 eq.) were dissolved in 5 mL of DMF in a 10 mL Schleck flask. The flask was purged with a stream of N_2, DIPEA (200 µL, 1.2 mmol, 20 eq.) was added, and the reaction mixture was stirred at RT for 24 h under argon. Later on, 5 mL of EtOH were added to the mixture, the flask was washed with further 10 mL of EtOH and the crude was finally purified by dialysis (3.5 kDa MWCO) in EtOH for 48 h. After dialysis, the solution was filtered through a 0.45 µm filter (Chromafil® PTFE), and the solvent was removed under reduced pressure yielding *l*-PMCPOXA-BCLA (490 mg, 88% yield) as a yellow viscous solid. The chemical structure and the purity of the synthesized polymer were determined by ^{1}H-NMR (500 MHz) (Figure S17).

Synthesis of l-PCPOXA (Figure S5, step iii)

To a solution of *l*-PMCPOXA-BCLA (200 mg, 1.1 mmol of CO_2H groups, 1 eq.) in EtOH (2 mL) 4 mL of 1 M NaOH (4.0 mmol, 3.6 eq.) solution were added, and the obtained mixture was stirred at RT for 24 h. The pH of the solution was neutralized with 1M HCl and the polymer

was subsequently purified by dialysis (3.5 kDa MWCO) in water for 24 h. The solution was passed through a 0.2 μm filter (Spartan 13/0.2 RC, Whatman®) and finally freeze-dried obtaining *l*-PCPOXA (170 mg, 94% yield) as a light yellow powder. The chemical structure and purity of *l*-PCPOXA were determined by ^{1}H-NMR (500 MHz) (Figure S18).

Synthesis of l-PGalaPOXA (Figure S5, step iv)

l-PCPOXA (100 mg, 0.6 mmol of CO_2H groups, 1 eq.) and galactosamine HCl (390 mg, 1.8 mmol, 3 eq.) were dissolved in 5 mL of MES buffer (150 mM). EDC-HCl (230 mg, 1.2 mmol, 2 eq.) in 1 mL of H_2O was added dropwise to the reaction mixture at RT, and the solution was left stirring for 24 h. After this time, the polymer was purified by dialysis (3.5 kDa MWCO) in H_2O for 48 h, and finally freeze-dried to yield *l*-PGalaPOXA (130 mg, 90% yield) as a slightly yellow powder. The chemical structure and the purity of *l*-PGalaPOXA was determined by ^{1}H-NMR (500 MHz) (Figure S19), and by aqueous SEC (Figure S26).

Synthesis of α-alkyne-ω-azide poly(2-methoxycarbonylpropyl-2-oxazoline) (PMCPOXA) (Figure S6, step i)

To an oven-dried 50 mL Schleck flask dry ACN (13 mL) and MCPOXA (6.44 g, 37.6 mmol, 50 eq.) were added under N_2. Propargyl tosylate (158 mg, 0.8 mmol, 1 eq.) was added to the mixture at RT under N_2, and the solution was stirred for additional 10 min before the polymerization mixture was heated to 80 °C and stirred for 16 h under argon. Simultaneously, 3-azidopropylamine was stirred overnight in dry ACN over BaO at RT. The polymerization was terminated by adding an excess of 3-azidopropylamine (750 mg, 7.5 mmol, 10 eq.) through a filter (0.45 μm, Chromafil®, PTFE), and the mixture was left stirring for additional 48 h under argon. The solvent was removed under reduced pressure, and the crude polymer was precipitated three times from DCM in Et_2O. The polymer was dried under high vacuum to yield α-alkyne-ω-azide PMCPOXA (5.5 g, 85% yield) as a white viscous polymer. The chemical

structure and the purity of the synthesized polymer were determined by ^{1}H-NMR (500 MHz) (Figure S20). SEC analysis (Figure S25) provided M_n = 8000, M_w = 10100 and $Đ$ = 1.26.

Synthesis of cyclic-PMCPOXA (Figure S6, step ii)

Cyclic-PMCPOXA was synthesized by intramolecular ring-closure method *via* copper(I)-catalyzed alkyne-azide cycloaddition of α-alkyne-ω-azide PMCPOXA under high dilution. α-alkyne-ω-azide PMCPOXA (400 mg, 0.05 mmol, 1 eq.) was dissolved in 200 mL of DCM, and in a separate round-bottom flask PMDETA (700 µL, 3.4 mmol, 68 eq.) was dissolved in 1.2 L of DCM. The two solutions were deoxygenated by argon bubbling for 30 min. After this time, Cu(I)Br (400 mg, 2.8 mmol, 56 eq.) was added to the solution of PMDETA, and the two flasks were bubbled with argon for other 30 min. The degassing process was stopped and the solution of α-alkyne-ω-azide PMCPOXA was slowly added to the PMDETA/Cu(I)Br mixture over 48 h, using a high-precision tubing pump (IPC-N4, ISMATEC, Switzerland) at a rate of 45 µL min^{-1} at RT under an argon atmosphere. When the addition was completed, the reaction was kept under argon and stirred for additional 24 h. The volume of the obtained mixture was reduced to 100 mL, and it was stirred for 2 h with 150 mL of saturated solution of NH_4Cl. The two phases were separated and the organic layer was washed once with saturated NH_4Cl, dried with $MgSO_4$ and filtered. Residual copper was removed using a plug of basic alumina (Ecochrom™ Alumina B Activity: I, VWR) eluting with DCM. Cyclic-PMCPOXA was obtained after solvent removal as a light yellow polymer (320 mg, 80% yield). ^{1}H-NMR spectroscopy showed the disappearance of the peaks at δ = 4.05 – 4.10 ppm (denoted as l in Figure S20) corresponding to the two protons at the alpha terminus in the linear precursor (α-alkyne-ω-azide PMCPOXA). Additionally, a new peak appeared at δ = 8.05 ppm (denoted as j in Figure S21), corresponding to the proton of the 1,2,3-triazole heterocycle that characterized the cyclized product (cyclic-PMCPOXA). SEC analysis showed a slight but significant shift to

larger retention volume (RV) in the cyclic-PMCPOXA with respect to its linear precursor (Figure S25). This shift to higher RV is typically observed for a successful cyclization reaction. Moreover, FT-IR spectroscopy confirmed the formation of the cyclic product (Figure S27).

Synthesis of c-PMCPOXA-BCLA (Figure S6, step iii)

Cyclic-PMCPOXA (235 mg, 0.03 mmol of secondary amine groups, 1 eq.), BCLA (50 mg, 0.15 mmol. 5 eq.) and COMU (70 mg, 0.17 mmol, 5.5 eq.) were dissolved in 3 mL of DMF in a 10 mL Schleck flask. The mixture was purged with a stream of N_2, DIPEA (100 uL, 0.6 mmol, 20 eq.) was added, and reaction mixture was stirred at RT for 24 h under argon. Subsequently, 15 mL of EtOH were added to the solution, and the mixture was purified by dialysis (3.5 kDa MWCO) in EtOH for 48 h. After dialysis, the solution was passed through a 0.45 µm filter (Chromafil® PTFE), and the solvent was removed to yield *c*-PMCPOXA-BCLA (215 mg, 90% yield) as a yellow viscous polymer. The chemical structure and the purity of the synthesized polymer was determined by ^{1}H-NMR (500 MHz) (Figure S22).

Synthesis of c-PCPOXA (Figure S6, step iv)

The synthesis of *c*-PCPOXA was performed similarly to that of *l*-PCPOXA. The chemical structure and purity of *c*-PCPOXA were determined by ^{1}H-NMR (500 MHz) (Figure S23).

Synthesis of c-PGalaPOXA (Figure S6, step v)

The synthesis of *c*-PGalaPOXA was performed similarly to that of *l*-PGalaPOXA. The chemical structure and purity of *c*-PGalaPOXA were determined by ^{1}H-NMR (500 MHz) (Figure S24).

AUTHOR INFORMATION

Corresponding Authors

nicholas.spencer@mat.ethz.ch

shivaprakash.ramakrishna@mat.ethz.ch

edmondo.benetti@mat.ethz.ch

Author Contributions

The manuscript was written through contributions of all authors. All authors have given approval to the final version of the manuscript.

ACKNOWLEDGMENTS

This work was financially supported by the Swiss National Science Foundation (CR32I3_166052). We thank Prof. Katharina Maniura (Empa) for the valuable discussions.

ASSOCIATED CONTENT

Supporting Information. Reaction schemes, NMR and FT-IR spectra, SEC elugrams. This material is available free of charge *via* the Internet at http://pubs.acs.org.

REFERENCES

1. Laurent, B. A.; Grayson, S. M., An Efficient Route to Well-Defined Macrocyclic Polymers *via* "Click" Cyclization. *J. Am. Chem. Soc.* **2006,** *128*, 4238-4239.
2. Laurent, B. A.; Grayson, S. M., Synthetic Approaches for the Preparation of Cyclic Polymers. *Chem. Soc. Rev.* **2009,** *38*, 2202-2213.
3. Josse, T.; De Winter, J.; Gerbaux, P.; Coulembier, O., Cyclic Polymers by Ring-Closure Strategies. *Angew. Chem. Int. Ed.* **2016,** *55*, 13944-13958.
4. Roland, C. D.; Li, H.; Abboud, K. A.; Wagener, K. B.; Veige, A. S., Cyclic Polymers from Alkynes. *Nat. Chem.* **2016,** *8*, 791-796.

5. Chang, Y. A.; Waymouth, R. M., Recent Progress on the Synthesis of Cyclic Polymers *via* Ring-Expansion Strategies. *J. Polym. Sci. Pol. Chem.* **2017,** *55*, 2892-2902.

6. Brown, H. A.; Waymouth, R. M., Zwitterionic Ring-Opening Polymerization for the Synthesis of High Molecular Weight Cyclic Polymers. *Acc. Chem. Res.* **2013,** *46*, 2585-2596.

7. Nadif, S. S.; Kubo, T.; Gonsales, S. A.; VenkatRamani, S.; Ghiviriga, I.; Sumerlin, B. S.; Veige, A. S., Introducing "Ynene" Metathesis: Ring-Expansion Metathesis Polymerization Leads to Highly Cis and Syndiotactic Cyclic Polymers of Norbornene. *J. Am. Chem. Soc.* **2016,** *138*, 6408-6411.

8. Niu, W. J.; Gonsales, S. A.; Kubo, T.; Bentz, K. C.; Pal, D.; Savin, D. A.; Sumerlin, B. S.; Veige, A. S., Polypropylene: Now Available without Chain Ends. *Chem* **2019,** *5*, 237-244.

9. Hadziioannou, G.; Cotts, P. M.; Tenbrinke, G.; Han, C. C.; Lutz, P.; Strazielle, C.; Rempp, P.; Kovacs, A. J., Thermodynamic and Hydrodynamic Properties of Dilute-Solutions of Cyclic and Linear Polystyrenes. *Macromolecules* **1987,** *20*, 493-497.

10. Arrighi, V.; Gagliardi, S.; Dagger, A. C.; Semlyen, J. A.; Higgins, J. S.; Shenton, M. J., Conformation of Cyclics and Linear Chain Polymers in Bulk by SANS. *Macromolecules* **2004,** *37*, 8057-8065.

11. Beaucage, G.; Kulkarni, A. S., Dimensional Description of Cyclic Macromolecules. *Macromolecules* **2010,** *43*, 532-537.

12. Magerl, D.; Philipp, M.; Metwalli, E.; Gutfreund, P.; Qiu, X. P.; Winnik, F. M.; Muller-Buschbaum, P., Influence of Confinement on the Chain Conformation of Cyclic Poly(N-isopropylacrylamide). *ACS Macro Lett.* **2015,** *4*, 1362-1365.

13. Kapnistos, M.; Lang, M.; Vlassopoulos, D.; Pyckhout-Hintzen, W.; Richter, D.; Cho, D.; Chang, T.; Rubinstein, M., Unexpected Power-Law Stress Relaxation of Entangled Ring Polymers. *Nat. Mater.* **2008,** *7*, 997-1002.

14. Jang, S. S.; Cagin, T.; Goddard, W. A., Effect of Cyclic Chain Architecture on Properties of Dilute Solutions of Polyethylene from Molecular Dynamics Simulations. *J. Chem. Phys.* **2003,** *119*, 1843-1854.

15. Yamamoto, T.; Tezuka, Y., Cyclic Polymers Revealing Topology Effects Upon Self-Assemblies, Dynamics and Responses. *Soft Matter* **2015,** *11*, 7458-7468.

16. Duval, M.; Lutz, P.; Strazielle, C., Hydrodynamic Dimensions of Ring-Shaped Macromolecules in a Good Solvent. *Makromol. Chem. Rapid Commun.* **1985,** *6*, 71-76.

17. Roovers, J., Dilute-Solution Properties of Ring Polystyrenes. *J. Polym. Sci. Pol. Phys.* **1985,** *23*, 1117-1126.

18. Yamamoto, T., Synthesis of Cyclic Polymers and Topology Effects on Their Diffusion and Thermal Properties. *Polym. J.* **2013,** *45*, 711-717.

19. Benetti, E. M.; Divandari, M.; Ramakrishna, S. N.; Morgese, G.; Yan, W. Q.; Trachsel, L., Loops and Cycles at Surfaces: The Unique Properties of Topological Polymer Brushes. *Chem. Eur. J.* **2017,** *23*, 12433-12442.

20. Morgese, G.; Trachsel, M.; Romio, M.; Divandari, M.; Ramakrishna, S. N.; Benetti, E. M., Topological Polymer Chemistry Enters Surface Science: Linear *versus* Cyclic Polymer Brushes. *Angew. Chem. Int. Ed.* **2016,** *55*, 15583 –15588

21. Divandari, M.; Morgese, G.; Trachsel, L.; Romio, M.; Dehghani, E. S.; Rosenboom, J. G.; Paradisi, C.; Zenobi-Wong, M.; Ramakrishna, S. N.; Benetti, E. M., Topology Effects on the Structural and Physicochemical Properties of Polymer Brushes. *Macromolecules* **2017,** *50*, 7760-7769.

22. Divandari, M.; Trachsel, L.; Yan, W. Q.; Rosenboom, J. G.; Spencer, N. D.; Zenobi-Wong, M.; Morgese, G.; Ramakrishna, S. N.; Benetti, E. M., Surface Density Variation within Cyclic Polymer Brushes Reveals Topology Effects on Their Nanotribological and Biopassive Properties. *ACS Macro Lett.* **2018,** *7*, 1455-1460.

23. Morgese, G.; Cavalli, E.; Rosenboom, J. G.; Zenobi-Wong, M.; Benetti, E. M., Cyclic Polymer Grafts That Lubricate and Protect Damaged Cartilage. *Angew. Chem. Int. Ed.* **2018,** *57*, 1621-1626.

24. Ramakrishna, S. N.; Morgese, G.; Zenobi-Wong, M.; Benetti, E. M., Comblike Polymers with Topologically Different Side Chains for Surface Modification: Assembly Process and Interfacial Physicochemical Properties. *Macromolecules* **2019,** *52*, 1632-1641.

25. Morgese, G.; Shaghasemi, B. S.; Causin, V.; Zenobi-Wong, M.; Ramakrishna, S. N.; Reimhult, E.; Benetti, E. M., Next-Generation Polymer Shells for Inorganic Nanoparticles are Highly Compact, Ultra-Dense, and Long-Lasting Cyclic Brushes. *Angew. Chem. Int. Ed.* **2017,** *56*, 4507-4511.

26. Minko, S., Responsive Polymer Brushes. *Polym. Rev.* **2006,** *46*, 397-420.

27. Hossain, M. D.; Reid, J. C.; Lu, D. R.; Jia, Z. F.; Searles, D. J.; Monteiro, M. J., Influence of Constraints within a Cyclic Polymer on Solution Properties. *Biomacromolecules* **2018,** *19*, 616-625.

28. Badoux, M.; Billing, M.; Klok, H. A., Polymer Brush Interfaces for Protein Biosensing Prepared by Surface-Iinitiated Controlled Radical Polymerization. *Polym. Chem.* **2019,** *10*, 2925-2951.

29. Satokawa, Y.; Shikata, T.; Tanaka, F.; Qiu, X. P.; Winnik, F. M., Hydration and Dynamic Behavior of a Cyclic Poly(N-isopropylacrylamide) in Aqueous Solution: Effects of the Polymer Chain Topology. *Macromolecules* **2009,** *42*, 1400-1403.

30. Qiu, X. P.; Tanaka, F.; Winnik, F. M., Temperature-Induced Phase Transition of Well-Defined Cyclic Poly(N-isopropylacrylamide)s in Aqueous Solution. *Macromolecules* **2007,** *40*, 7069-7071.

31. Xu, J.; Ye, J.; Liu, S. Y., Synthesis of Well-Defined Cyclic Poly(N-isopropylacrylamide) *via* Click Chemistry and Its Unique Thermal Phase Transition Behavior. *Macromolecules* **2007,** *40*, 9103-9110.

32. Yang, J.; Yamato, M.; Kohno, C.; Nishimoto, A.; Sekine, H.; Fukai, F.; Okano, T., Cell Sheet Engineering: Recreating Tissues without Biodegradable Scaffolds. *Biomaterials* **2005,** *26*, 6415-6422.

33. Takahashi, H.; Nakayama, M.; Yamato, M.; Okano, T., Controlled Chain Length and Graft Density of Thermoresponsive Polymer Brushes for Optimizing Cell Sheet Harvest. *Biomacromolecules* **2010,** *11*, 1991-1999.

34. Klein Gunnewiek, M.; Di Luca, A.; Bollemaat, H. Z.; van Blitterswijk, C. A.; Vancso, G. J.; Moroni, L.; Benetti, E. M., Creeping Proteins in Microporous Structures: Polymer Brush-Assisted Fabrication of 3D Gradients for Tissue Engineering. *Adv. Health. Mater.* **2015,** *4*, 1169–1174.

35. Kang, C. J.; Ramakrishna, S. N.; Nelson, A.; Cremmel, C. V. M.; Stein, H. V.; Spencer, N. D.; Isa, L.; Benetti, E. M., Ultrathin, Freestanding, Stimuli-Responsive, Porous Membranes from Polymer Hydrogel-Bbrushes. *Nanoscale* **2015,** *7*, 13017-13025.

36. de Groot, G. W.; Santonicola, M. G.; Sugihara, K.; Zambelli, T.; Reimhult, E.; Voros, J.; Vancso, G. J., Switching Transport through Nanopores with pH-Responsive Polymer Brushes for Controlled Ion Permeability. *ACS Appl. Mater. Interfaces* **2013,** *5*, 1400-1407.

37. Motornov, M.; Sheparovych, R.; Katz, E.; Minko, S., Chemical Gating with Nanostructured Responsive Polymer Brushes: Mixed Brush *versus* Homopolymer Brush. *ACS Nano* **2008,** *2*, 41-52.

38. Tokareva, I.; Minko, S.; Fendler, J. H.; Hutter, E., Nanosensors Based on Responsive Polymer Brushes and Gold Nanoparticle Enhanced Transmission Surface Plasmon Resonance Spectroscopy. *J. Am. Chem. Soc.* **2004,** *126*, 15950-15951.

39. Tokarev, I.; Tokareva, I.; Minko, S., Optical Nanosensor Platform Operating in Near-Physiological pH Range *via* Polymer-Brush-Mediated Plasmon Coupling. *ACS Appl. Mater. Interfaces* **2011,** *3*, 143-146.

40. Tagit, O.; Tomczak, N.; Benetti, E. M.; Cesa, Y.; Blum, C.; Subramaniam, V.; Herek, J. L.; Vancso, G. J., Temperature-Modulated Quenching of Quantum Dots Covalently Coupled to Chain Ends of Poly(N-isopropyl acrylamide) Brushes on Gold. *Nanotechnology* **2009,** *20*, 185501.

41. Verbraeken, B.; Monnery, B. D.; Lava, K.; Hoogenboom, R., The Chemistry of Poly(2-oxazoline)s. *Eur. Polym. J.* **2017,** *88*, 451-469.

42. Bouten, P. J. M.; Hertsen, D.; Vergaelen, M.; Monnery, B. D.; Boerman, M. A.; Goossens, H.; Catak, S.; van Hest, J. C. M.; Van Speybroeck, V.; Hoogenboom, R., Accelerated Living Cationic Ring-Opening Polymerization of a Methyl Ester Functionalized 2-Oxazoline Monomer. *Polym. Chem.* **2015,** *6*, 514-518.

43. Sehlinger, A.; Verbraeken, B.; Meier, M. A. R.; Hoogenboom, R., Versatile Side Chain Modification *via* Isocyanide-Based Multicomponent Reactions: Tuning the LCST of Poly(2-oxazoline)s. *Polym. Chem.* **2015,** *6*, 3828-3836.

44. Lundquist, J. J.; Toone, E. J., The Cluster Glycoside Effect. *Chem. Rev.* **2002,** *102*, 555-578.

45. Becer, C. R., The Glycopolymer Code: Synthesis of Glycopolymers and Multivalent Carbohydrate-Lectin Interactions. *Macromol. Rapid Commun.* **2012,** *33*, 742-752.

46. Willey, T. M.; Vance, A. L.; Bostedt, C.; van Buuren, T.; Meulenberg, R. W.; Terminello, L. J.; Fadley, C. S., Surface Structure and Chemical Switching of Thioctic Acid Adsorbed on Au(111) as Observed Using Near-edge X-ray Absorption Fine Structure. *Langmuir* **2004,** *20*, 4939-4944.

47. Yan, W. Q.; Divandari, M.; Rosenboom, J. G.; Ramakrishna, S. N.; Trachsel, L.; Spencer, N. D.; Morgese, G.; Benetti, E. M., Design and Characterization of Ultrastable, Biopassive and Lubricious Cyclic Poly(2-alkyl-2-oxazoline) Brushes. *Polym. Chem.* **2018,** *9*, 2580-2589.

48. Gillich, T.; Benetti, E. M.; Rakhmatullina, E.; Konradi, R.; Li, W.; Zhang, A.; Schluter, A. D.; Textor, M., Self-Assembly of Focal Point Oligo-catechol Ethylene Glycol Dendrons on Titanium Oxide Surfaces: Adsorption Kinetics, Surface Characterization, and Nonfouling Properties. *J. Am. Chem. Soc.* **2011,** *133*, 10940-10950.

49. Zhulina, E. B.; Birshtein, T. M.; Borisov, O. V., Theory of Ionizable Polymer Brushes. *Macromolecules* **1995,** *28*, 1491-1499.

50. Currie, E. P. K.; Sieval, A. B.; Fleer, G. J.; Stuart, M. A. C., Polyacrylic Acid Brushes: Surface Pressure and Salt-induced Swelling. *Langmuir* **2000,** *16*, 8324-8333.

51. Biesalski, M.; Johannsmann, D.; Ruhe, J., Synthesis and Swelling Behavior of a Weak Polyacid Brush. *J. Chem. Phys.* **2002,** *117*, 4988-4994.

52. Gong, P.; Wu, T.; Genzer, J.; Szleifer, I., Behavior of Surface-anchored Poly(acrylic acid) Brushes with Grafting Density Gradients on Solid Substrates: 2. Theory. *Macromolecules* **2007,** *40*, 8765-8773.

53. Wu, T.; Gong, P.; Szleifer, I.; Vlcek, P.; Subr, V.; Genzer, J., Behavior of Surface-Anchored Poly(acrylic acid) Brushes with Grafting Density Gradients on Solid Substrates: 1. Experiment. *Macromolecules* **2007,** *40*, 8756-8764.

54. Miao, Z. H.; Kubo, T.; Pal, D.; Sumerlin, B. S.; Veige, A. S., pH-Responsive Water-Soluble Cyclic Polymer. *Macromolecules* **2019,** *52*, 6260-6265.

55. Benetti, E. M.; Reimhult, E.; de Bruin, J.; Zapotoczny, S.; Textor, M.; Vancso, G. J., Poly(methacrylic acid) Grafts Grown from Designer Surfaces: The Effect of Initiator Coverage on Polymerization Kinetics, Morphology, and Properties. *Macromolecules* **2009,** *42*, 1640-1647.

56. Raftari, M.; Zhang, Z. J.; Carter, S. R.; Leggett, G. J.; Geoghegan, M., Nanoscale Contact Mechanics between Two Grafted Polyelectrolyte Surfaces. *Macromolecules* **2015,** *48*, 6272-6279.

57. Gunnewiek, M. K.; Ramakrishna, S. N.; di Luca, A.; Vancso, G. J.; Moroni, L.; Benetti, E. M., Stem-Cell Clinging by a Thread: AFM Measure of Polymer-Brush Lateral Deformation. *Adv. Mater. Interfaces* **2016,** *3*, 1500456.

58. Dehghani, E. S.; Spencer, N. D.; Ramakrishna, S. N.; Benetti, E. M., Crosslinking Polymer Brushes with Ethylene Glycol-Containing Segments: Influence on Physicochemical and Antifouling Properties. *Langmuir* **2016,** *32*, 10317-10327.

59. Raviv, U.; Giasson, S.; Kampf, N.; Gohy, J. F.; Jerome, R.; Klein, J., Lubrication by Charged Polymers. *Nature* **2003,** *425*, 163-165.

60. Cairo, C. W.; Gestwicki, J. E.; Kanai, M.; Kiessling, L. L., Control of Multivalent Interactions by Binding Epitope Density. *J. Am. Chem. Soc.* **2002,** *124*, 1615-1619.

61. Lavilla, C.; Yilmaz, G.; Uzunova, V.; Napier, R.; Becer, C. R.; Heise, A., Block-Sequence-Specific Glycopolypeptides with Selective Lectin Binding Properties. *Biomacromolecules* **2017,** *18*, 1928-1936.

62. Jono, K.; Nagao, M.; Oh, T.; Sonoda, S.; Hoshino, Y.; Miura, Y., Controlling the Lectin Recognition of Glycopolymers *via* Distance Arrangement of Sugar Blocks. *Chem. Commun.* **2018,** *54*, 82-85.

63. Becer, C. R.; Gibson, M. I.; Geng, J.; Ilyas, R.; Wallis, R.; Mitchell, D. A.; Haddleton, D. M., High-Affinity Glycopolymer Binding to Human DC-SIGN and Disruption of DC-SIGN Interactions with HIV Envelope Glycoprotein. *J. Am. Chem. Soc.* **2010,** *132*, 15130-15132.

64. Ponader, D.; Wojcik, F.; Beceren-Braun, F.; Dernedde, J.; Hartmann, L., Sequence-Defined Glycopolymer Segments Presenting Mannose: Synthesis and Lectin Binding Affinity. *Biomacromolecules* **2012,** *13*, 1845-1852.

65. Chen, Y.; Lord, M. S.; Piloni, A.; Stenzel, M. H., Correlation between Molecular Weight and Branch Structure of Glycopolymers Stars and Their Binding to Lectins. *Macromolecules* **2015,** *48*, 346-357.

66. Lin, K.; Kasko, A. M., Effect of Branching Density on Avidity of Hyperbranched Glycomimetics for Mannose Binding Lectin. *Biomacromolecules* **2013,** *14*, 350-357.

67. Chen, Y.; Chen, G. J.; Stenzel, M. H., Synthesis and Lectin Recognition of Glyco Star Polymers Prepared by "Clicking" Thiocarbohydrates onto a Reactive Scaffold. *Macromolecules* **2010,** *43*, 8109-8114.

68. Fasting, C.; Schalley, C. A.; Weber, M.; Seitz, O.; Hecht, S.; Koksch, B.; Dernedde, J.; Graf, C.; Knapp, E. W.; Haag, R., Multivalency as a Chemical Organization and Action Principle. *Angew. Chem. Int. Ed.* **2012,** *51*, 10472-10498.

69. Zhang, Q.; Su, L.; Collins, J.; Chen, G. S.; Wallis, R.; Mitchell, D. A.; Haddleton, D. M.; Becer, C. R., Dendritic Cell Lectin-Targeting Sentinel-like Unimolecular Glycoconjugates To Release an Anti-HIV Drug. *J. Am. Chem. Soc.* **2014,** *136*, 4325-4332.

70. Sastry, M. V. K.; Banarjee, P.; Patanjali, S. R.; Swamy, M. J.; Swarnalatha, G. V.; Surolia, A., Analysis of Saccharide Binding to Artocarpus-Integrifolia Lectin Reveals Specific Recognition of T-Antigen (Beta-D-Gal(1-]3)D-Galnac). *J. Biol. Chem.* **1986,** *261*, 1726-1733.

71. Bourne, Y.; Astoul, C. H.; Zamboni, V.; Peumans, W. J.; Menu-Bouaouiche, L.; Van Damme, E. J. M.; Barre, A.; Rouge, P., Structural Basis for the Unusual Carbohydrate-Binding Specificity of Jacalin Towards Galactose and Mannose. *Biochem. J.* **2002,** *364*, 173-180.

72. Yilmaz, G.; Uzunova, V.; Napier, R.; Becer, C. R., Single-Chain Glycopolymer Folding *via* Host-Guest Interactions and Its Unprecedented Effect on DC-SIGN Binding. *Biomacromolecules* **2018,** *19*, 3040-3047.

73. Reimhult, E.; Larsson, C.; Kasemo, B.; Höök, F., Simultaneous Surface Plasmon Resonance and Quartz Crystal Microbalance with Dissipation Monitoring Measurements of Biomolecular Adsorption Events Involving Structural Transformations and Variations in Coupled Water. *Anal. Chem.* **2004,** *76*, 7211-7220.

74. Hilfiker, J. N.; Synowicki, R. A.; Bungay, C. L.; Carpio, R. B. T.-S. S. T. Spectroscopic Ellipsometry for Polymer Thin Films. **1998**, *41*, 101.

75. Hutter, J. L.; Bechhoefer, J. Calibration of Atomic-Force Microscope Tips. *Rev. Sci. Instrum.* **1993**, *64*, 1868–1873.

76. Green, C. P.; Lioe, H.; Cleveland, J. P.; Proksch, R.; Mulvaney, P.; Sader, J. E. Normal and Torsional Spring Constants of Atomic Force Microscope Cantilevers. *Rev. Sci. Instrum.* **2004**, *75*, 1988–1996.

77. Cannara, R. J.; Eglin, M.; Carpick, R. W. Lateral Force Calibration in Atomic Force Microscopy: A New Lateral Force Calibration Method and General Guidelines for Optimization. *Rev. Sci. Instrum.* **2006**, *77*, 053701.

78. Bouten, P. J. M.; Hertsen, D.; Vergaelen, M.; Monnery, B. D.; Catak, S.; Van Hest, J. C. M.; Van Speybroeck, V.; Hoogenboom, R. Synthesis of Poly(2-Oxazoline)s with Side Chain Methyl Ester Functionalities: Detailed Understanding of Living Copolymerization Behavior of Methyl Ester Containing Monomers with 2-Alkyl-2-Oxazolines. *J. Polym. Sci.* **2015**, *53*, 2649–2661.

For Table of Contents Use Only:

Functional Nanoassemblies of Cyclic Polymers Show Amplified Responsiveness and Enhanced Protein-Binding Ability

Lucca Trachsel, Matteo Romio, Benjamin Grob, Marcy Zenobi-Wong, Nicholas D. Spencer, Shivaprakash N. Ramakrishna, Edmondo M. Benetti